Shelving Spectroscopy and Atomic Clock Development of the Strontium 689 nm Intercombination Line

by

Samuel James Porter

April 5th, 2023

A thesis submitted to the

Faculty of the College of Arts and Sciences of the

University of Colorado in partial fulfillment

of the requirements for Latin Honors in the

Department of Physics

2023

Committee Members:

Dr. John Kitching, Physics, Advisor

Dr. Paul Beale, Physics

Dr. Akira Miyake, Psychology

Porter, Samuel James (BA Physics, Psychology, Mathematics)

Shelving Spectroscopy and Atomic Clock Development of the Strontium 689 nm Intercombination Line

Precise timekeeping is crucial for a myriad of applications, including GPS, telecommunications, financial transaction time-stamping, and more [20]. The burgeoning demand for increasingly accurate clocks at a smaller scale has driven significant progress in atomic clock miniaturization over the past two decades [8][10]. Chip-scale atomic clocks have emerged by employing micro-fabricated vapor cells containing atomic species conducive to high-precision timekeeping [20][12].

Strontium has emerged as an exceptional candidate for atomic clocks, with the development of clocks exhibiting deviations of less than 1 second in 300 billion years [5]. However, a chip-scale strontium clock remains to be realized.

This paper delineates the advancements made toward the development of a strontium atomic clock utilizing a micro-fabricated vapor cell. The proposed design involves implementing a shelving spectroscopy scheme that employs the $^1S_0$-$^3P_1$ transition as the clock transition. Further refinement of the shelving scheme and the associated laser lock systems is necessary prior to the establishment of a functional clock. All components of this proposed design, encompassing both optical and electrical elements, can be miniaturized to chip scale, rendering it a promising solution for a wide range of applications with stringent weight and volume constraints.

The strontium clock design outlined in this paper incorporates frequency and phase lock systems, which are critical for achieving precise resonance between the shelving and intermediate lasers with their respective transitions. This paper discusses the current limitations of these locking systems and proposes potential improvements. Once the frequency and phase locks are optimized and an additional frequency lock is employed, a clock is created by pairing a frequency counter with the laser resonant with the clock transition.

Dedication

To Mom and Dad, for tolerating me.

Acknowledgements

I would like to express my appreciation to Dr. Matthew Hummon and Dr. Yang Li for their continual guidance throughout my time at NIST. This experience has been immensely educational because of their support. I would like to thank Dr. Matthew Hummon specifically for his continual kindness and patience, and for inviting me to join this great research team despite my inexperience. I would also like to thank Konrad Ziegler for inviting me to join him on a tour of NIST in March of 2022, which ultimately lead to my involvement in this project.

Contents

Chapter

Figures

Figure

Chapter 1

Clocks

Clocks are composed of two components, an oscillator and a counter. An oscillator, or frequency standard, is anything that repeats at a consistent interval. A counter is anything that can track, or count, each repetition of a frequency standard. One example of a clock is a grandfather clock. It consists of a pendulum, its frequency standard, and a gear, its counter. A pendulum is a good oscillator because, in an isolated environment, the period of a pendulum only depends on the acceleration due to gravity and the length of the pendulum 1.1.

$$\tau = 2\pi\sqrt{\frac{\ell}{g}} \tag{1.1}$$

The period τ is solely dependent on ℓ, the length of the pendulum, and g, the acceleration due to gravity. Each swing of a pendulum can be counted using a gear, thus converting the abstract quantity time into a physical quantity, angular rotation.

The quality of a clock is determined by the rate and consistency of its oscillator and the tallying ability of its counter. When compared to modern clocks, a grandfather clock has a low rate of oscillation, poor consistency, and mediocre tallying ability. Alternative oscillators and counters must be investigated for the development of high-quality clocks.

1.1 Light

Light satisfies the two criteria for a good oscillator. Its rate of oscillation, or frequency, is both high and consistent. Where the rate of oscillation for a grandfather clock is 1 Hz, the

rate of oscillation for visible light is between 400 THz and 800 THz. The frequency of light is also consistent. As we know from Einstein's special theory of relativity, the frequency of light is constant in the inertial frame of the source of light. The frequency of light, within an inertial frame, does not change when propagating through a linear medium, such as a vacuum or the atmosphere.

In order to generate light at a single frequency, we employ a laser as the source. The term "laser" is an acronym for Light Amplification by Stimulated Emission of Radiation. This device produces a highly focused beam of light with a narrow frequency range. The underlying mechanism behind laser operation is stimulated emission, a process in which a gain medium, such as a crystal, is induced to emit light.

Stimulated emission is initiated by applying an electric current to the gain medium. This current excites the atoms within the medium to energy levels above their ground state. A photon possessing the same energy as the difference between the excited and ground states is then introduced into the gain medium. Upon interacting with the excited atoms, the photon causes these atoms to decay to their ground state, consequently releasing a photon with an energy equivalent to the difference between the excited and ground states.

The released photons continue to interact with atoms in the gain medium, generating additional photons in the process. These photons are confined within a resonant cavity, allowing only those with a specific phase to propagate continuously. This cavity is constructed using two mirrors that repeatedly reflect the photons back through the gain medium, thereby producing numerous coherent photons, or photons with nearly identical frequency and phase.

Given that the laser's output consists of photons with nearly uniform frequency, it can serve as a highly precise oscillator for clock applications.

1.2 Measuring Light

What "gear" can we use to measure light? The highest frequency that can propagate electronically is approximately 36 GHz [6]. In contrast, optical frequencies, or frequencies of visible light, range from 400 THz to 800 THz. Therefore, measuring the electric component of an electromag-

netic wave is not directly possible with electronics. Nevertheless, this challenge can be mitigated by employing the superposition principle for electromagnetic fields. When electromagnetic waves coincide or superimpose, the resultant wave is the vector sum of the individual waves. For instance, consider the following waves 1.2, 1.3:

$$W_1 = A_1 \sin(2\pi f_1 t + \phi_1) \tag{1.2}$$

$$W_2 = A_2 \sin(2\pi f_2 t + \phi_2) \tag{1.3}$$

W_i is the function of each wave, f_i is the frequency of each wave, A_i is the amplitude of each wave, and ϕ_i is the phase of each wave. Superimposing W_1 and W_2 results in the following wave 1.4.

$$W_1 + W_2 = A_1 \sin(2\pi f_1 t + \phi_1) + A_2 \sin(2\pi f_2 t + \phi_2) \tag{1.4}$$

Simplifying further results in the following product 1.5.

$$W_1 + W_2 = 2A_1 A_2 \sin(\frac{1}{2}[2\pi(f_1 + f_2)t + (\phi_1 + \phi_2)]) \cdot \cos(\frac{1}{2}[2\pi(f_1 - f_2)t + (\phi_1 - \phi_2)]) \tag{1.5}$$

Figure 1.1 shows W_1 and W_2 and their sum, where the frequency of W_2 is 10% higher than that of W_1. The sum of waves W_1 and W_2 produces a carrier-envelope waveform. In Equation 1.5, the first factor is the formula for the carrier wave and the second factor is the formula for the envelope. Figure 1.2 depicts the carrier-envelope wave juxtaposed with its envelope.

$$W_{envelope} = 2A_1 A_2 \cos(\frac{1}{2}[2\pi(f_1 - f_2)t + (\phi_1 - \phi_2)]) \tag{1.6}$$

As shown in Equation 1.6, the frequency of the envelope is $\frac{1}{2}(f_1 - f_2)$, where f_1 is the frequency of W_1 and f_2 is the frequency of W_2. A photodiode (PD) is a semiconductor device, which efficiently transforms incident photons, or light, into electrical current. Photodiodes produce an electrical current proportional to the number of photons. For the carrier-envelope wave formed by the superposition of W_1 and W_2, the electrical frequency produced by a photodiode is called the beat note. Figure 1.3 shows the beat note produced by the carrier-envelope wave.

Figure 1.1: Superposition of Unequal Waves. Subplot (a) depicts wave W_1 in blue, subplot (b) depicts wave W_2 in red, and subplot (c) depicts the superposition wave $W_1 + W_2$ in magenta. The frequency of W_2 is 10% higher than that of W_1.

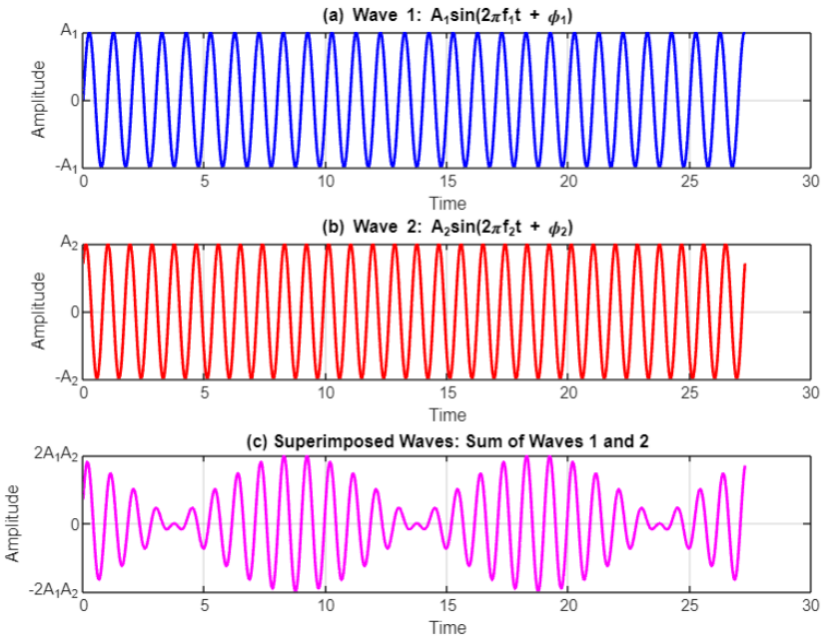

Figure 1.2: Carrier-envelope waveform with its envelope. Equation 1.6 is the formula for the envelope waveform, denoted in black. Equation 1.5 is the formula for the carrier-envelope waveform, denoted in magenta.

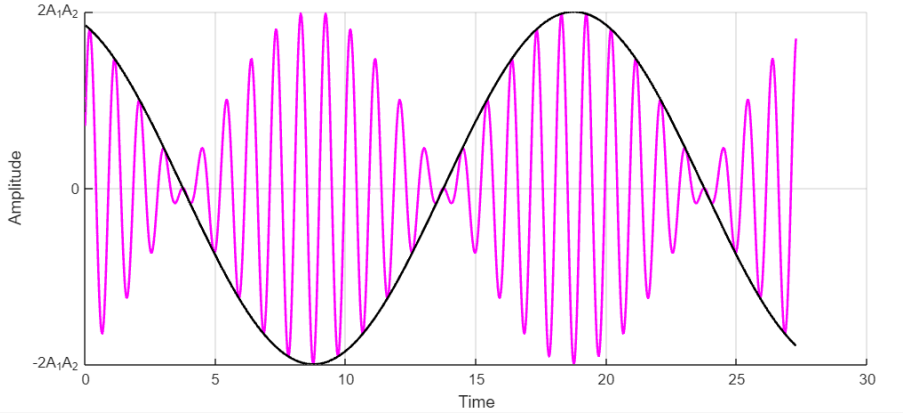

Figure 1.3: The carrier-envelope wave, denoted in magenta, and its beat note, denoted in black. The beat note has a frequency that is twice that of the envelope.

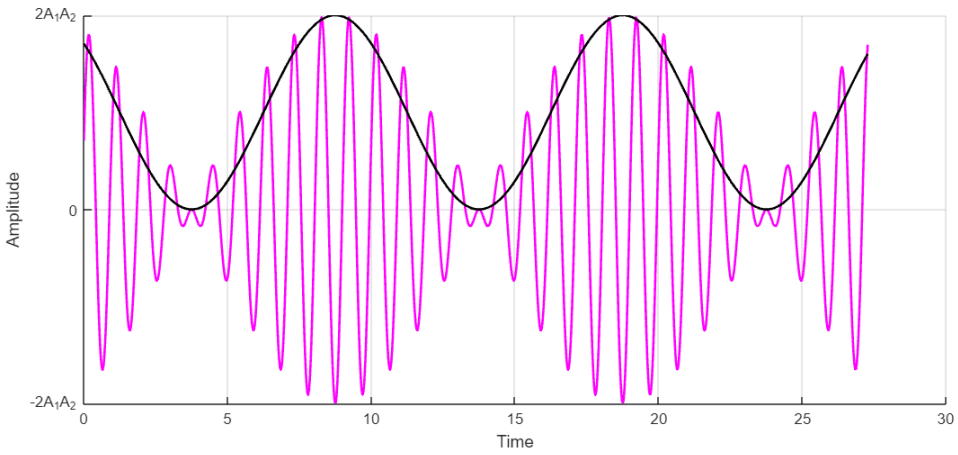

The frequency of the beat note is precisely twice that of the envelope, signifying that the beat note's frequency is the exact difference between the frequencies of waves W_1 and W_2. Provided that W_1 and W_2 exhibit a frequency difference less than 36 GHz, the beat note can propagate electronically, enabling it to be measured. Equation 1.7 offers an approximation for the electrical beat note.

$$W_{\text{beat note}} = A_1 A_2 \cos([2\pi(f_1 - f_2)t + (\phi_1 - \phi_2)] \tag{1.7}$$

Measuring a beat note allows for the accurate determination of an electromagnetic wave's frequency. Consider a reference electromagnetic wave with frequency f_r. By superimposing this reference wave with the wave we aim to measure, an electronic beat note with frequency f_b is generated. As f_b corresponds to the frequency difference between the reference wave and the wave to be measured, the frequency of the electromagnetic wave we seek to measure f_m can be computed using Equation 1.8.

$$f_m = f_r + f_b \tag{1.8}$$

1.2.1 Frequency Combs

In order to generate a reference optical signal that can be superimposed with the signal we aim to measure, we must address a key issue. The bandwidth of any given optical signal is 400 THz, which is significantly greater than the 36 GHz transmissible via electronics. Consequently, the difference between a specific optical reference and the signal we wish to measure is likely to exceed 36 GHz.

A viable solution to this problem is to generate multiple optical references with differences between each reference being less than the highest measurable signal. However, in many electronics, a 36 GHz measurement remains too high. For instance, the Siglent SSA3021X Spectrum Analyzer, an industry-standard tool for measuring radio frequency (RF) signals, has an upper limit of 2.1 GHz.

Therefore, numerous signals must be generated, with the difference between adjacent frequencies being less than 2.1 GHz. This ensures the generation of a beat note with a measurable frequency.

A pulsed laser can be employed to generate multiple signals at a fixed frequency difference. Pulsed lasers are characterized by their operation at fixed intervals, turning on and off periodically. Figure 1.4 below illustrates the waveform of a laser pulsed at a rate of f_{rep}.

Figure 1.4: Pulsed Laser Waveform. ϕ_0 is the phase difference between the carrier and the envelope for each pulse. f_{rep} is the repetition rate of the laser. T_{rep} is the period of the envelope. f_{CEO} is the frequency of the carrier-envelope offset. T_{CEO} is the period of ϕ_0. [22]

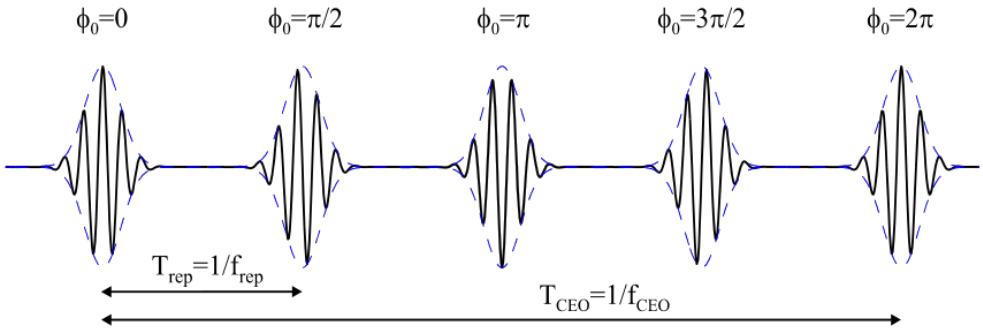

The pulsed laser wave is equivalent to the superposition wave generated by superimposing an infinite number of electromagnetic waves with a successive frequency difference of f_{rep}, as depicted in Figure 1.5 below.

By using a frequency comb to generate a beat note with an electromagnetic wave that we wish to measure, f_r in Equation 1.8 can be replaced with $f_{CEO} + nf_{rep}$, where f_{CEO} is the frequency of the carrier-envelope offset, f_{rep} is the frequency of the repetition rate, and n is the integer number of the comb tooth closest to the wave we wish to measure. Thus, Equation 1.8 becomes Equation **??**.

$$f_m = f_{CEO} + nf_{rep} + f_b \tag{1.9}$$

Therefore, the precise frequency of an electromagnetic wave can be calculated by producing a beat note between it and a frequency comb with a known carrier-envelope offset, known repetition rate, and known integer number of the tooth that is closest to the wave.

Figure 1.5: Frequency Comb Fourier Transform. Subplot (a) depicts the waveform of a pulsed laser. Subplot (b) depicts the output of a pulsed laser in the frequency domain. [18]

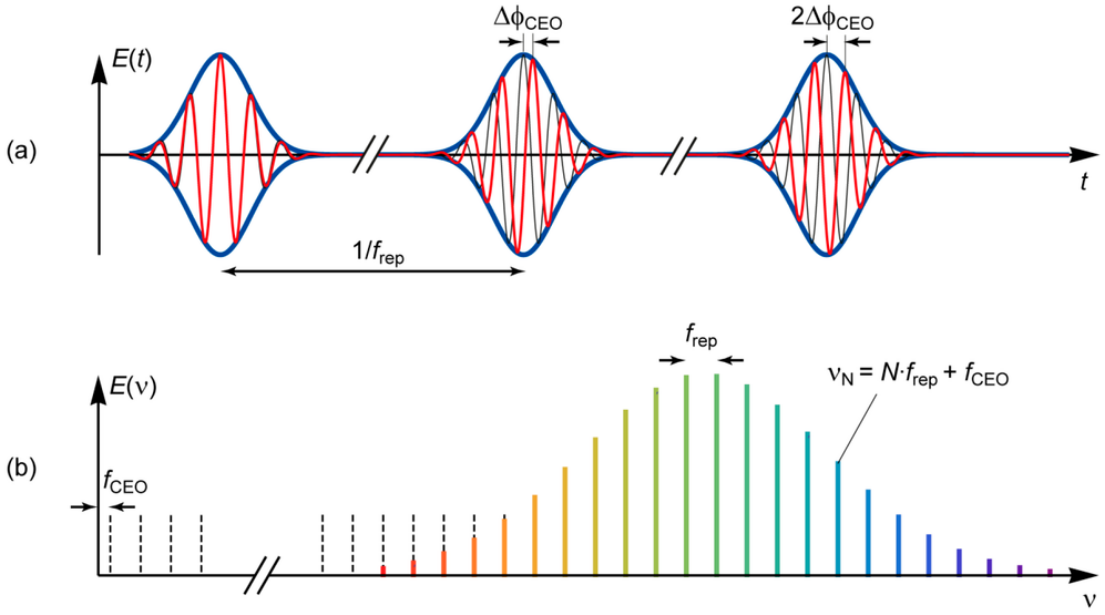

Chapter 2

Spectroscopy

So far, we have explored two crucial aspects of creating a clock. Firstly, the generation of a consistent oscillator via light produced by stimulated emission, and secondly, the process by which the frequency of light can be measured. Although the frequency of light emitted from a laser remains constant while propagating through free space, the laser-generated frequency may change due to environmental factors, such as temperature, pressure, and acoustic vibrations, which impact the stimulation of the gain medium. Given the sensitivity of lasers to environmental factors, it is essential to ensure consistent frequency emission. This can be achieved by utilizing spectroscopy techniques that leverage the electronic transitions of atoms.

2.1 Atomic Transitions

When a photon interacts with an atom, it may be absorbed. Upon absorption, a valence electron in the ground state is elevated to an excited state, where the difference in energy between the excited state and the ground state is equivalent to the photon's energy. The energy of a photon, determined solely by its frequency, allows us to deduce the photon's frequency when absorbed by an atom. The energy of a photon and its frequency are related by Equation 2.1.

$$E = hf \tag{2.1}$$

In Equation 2.1, E is the photon's energy, f is the photon's frequency, and h is Planck's constant, 6.63×10^{-34} Js. Resonance occurs when the energy of an incident photon matches the

energy difference of a transition, which increases the probability of the transition taking place.

The energy levels that electrons bound to an atom can occupy are quantized, meaning that the electron can only take on discrete values of energy. An electron is excited to a higher energy level when an atom absorbs a photon. Therefore, there are only discrete frequencies of photons that can be absorbed by an atom.

Electric dipole transitions in atoms are governed by a set of selection rules that describe the conditions under which a transition between two energy levels can occur. A transition is considered spin-forbidden if it involves a change in the total spin quantum number S, i.e., $\Delta S \neq 0$. Spin-forbidden transitions are often referred to as intercombination lines. Although intercombination lines are considered classically forbidden, they can still occur in quantum systems. This is because weak interactions that are not explicitly forbidden by conservation or symmetry laws can still contribute to transition probabilities. The weak interaction that allows for intercombination lines is called spin-orbit coupling. However, due to the weak effect of spin-orbit coupling, transitions that involve a change in spin are less likely to occur than transitions that do not involve a change in spin.

Since transitions that involve a change in spin are less likely to occur, they generally have a longer lifetime than transitions that do not involve a change in spin. The lifetime of an excited state is the length of time that an electron will generally stay in an excited state before decaying back to a lower state or the ground state. A longer lifetime corresponds to a lower transition probability, conversely, a shorter lifetime corresponds to a higher transition probability. As a result, transitions that involve a change in spin have a longer lifetime than those that do not.

The longevity of an excited state exhibits a correlation with the linewidth associated with the corresponding transition. The Heisenberg uncertainty principle reveals an inverse relationship between a quantum state's duration and the ambiguity in its energy. Consequently, a transition with an extended lifetime aligns with a more narrow linewidth, while a diminished lifetime corresponds to a more broad linewidth. The linewidth is the range of frequencies that can potentially induce a given transition. Consequently, transitions involving a change in spin exhibit a more restricted

linewidth due to their extended lifetimes.

2.2 Saturation Absorption Spectroscopy

Saturation absorption spectroscopy is a technique that enables precise determination of atomic transition frequencies by reducing the effects of Doppler broadening. This method involves the use of two counter-propagating laser beams: a pump beam and a probe beam. The pump beam is strong relative to the probe beam and is strong enough to saturate the absorption of the atomic sample. The probe beam is weaker than the pump beam and is used to measure the absorption spectrum.

Doppler broadening of atomic transitions is a phenomenon that occurs due to the Doppler effect. The Doppler effect is the change in frequency of a wave experienced by an observer that is moving relative to the source of the wave. In the context of atomic transitions, Doppler broadening arises because atoms in a gaseous medium occupy a distribution of velocities. As a result, the apparent frequency of the light absorbed or emitted by the atoms will shift according to their relative velocity with respect to an observer. This causes the atomic transition lines to become broadened because a greater range of frequencies will be absorbed or emitted. Doppler broadening is a critical factor in spectroscopy, as it can limit the precision of measurements.

Saturation absorption spectroscopy is used to ameliorate the effects of Doppler broadening. In saturation absorption spectroscopy, the pump and probe beams are counter-propagating. This means that beams are overlapped and propagate in opposite directions across the sample. This configuration ensures that an opposite Doppler shift is experienced by each beam. Atoms in the sample that experience a Doppler increase in frequency when interacting with the pump beam, will experience a Doppler decrease in frequency when interacting with the probe beam and vice versa. The probe beam will experience a reduction in absorption for atoms in the velocity class where the Doppler shifts for each beam cancels. This results in the observation of a narrow, Doppler-free spectral feature in the absorption spectrum.

As shown in Figure 2.1 below, the Doppler-free feature is detected as a decrease in absorp-

tion at the precise transition frequency. This Doppler-free feature, also known as a Lamb dip, is significantly narrower than the Doppler-broadened absorption profile.

Figure 2.1: (a) Example configuration of a saturation absorption scheme. (b) The absorption profile of an atomic transition measured by a photodiode [14].

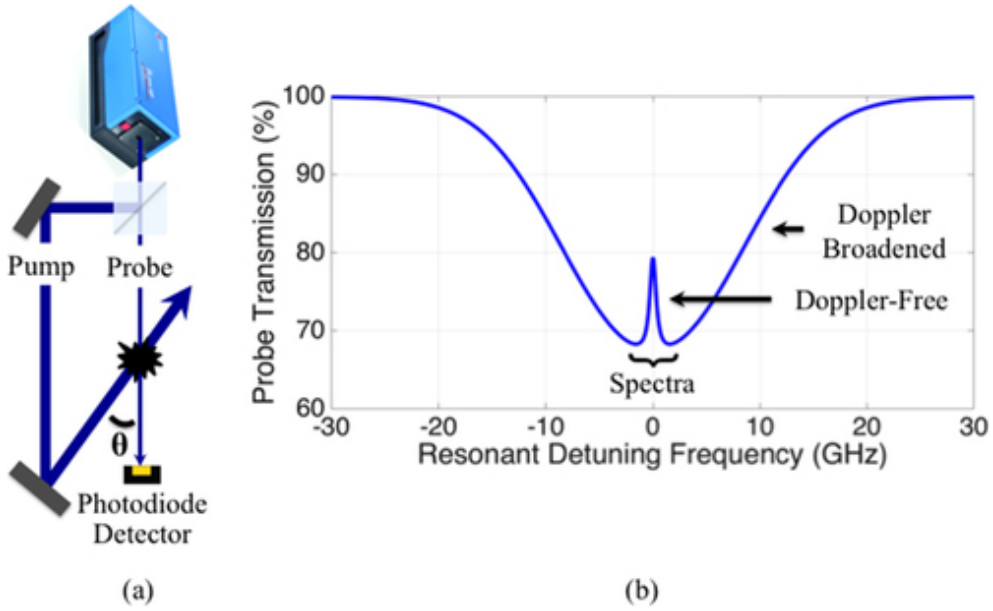

The Doppler-broadened profile shown in Figure 2.1 is typically generated by scanning the frequency of a laser. A scan is defined as a manipulation of the laser current that causes the laser frequency to pass over a broad range of frequencies, typically on the order of 10 GHz. The rate of the scan, or how fast the laser passes over the frequency range of the scan, is typically on the order of 10kHz. As the frequency produced by the laser approaches the precise transition frequency, the transmission of the beam through the interrogated sample decreases. Minimum transmission of the probe beam indicates maximum absorption by the sample, and thus the laser is briefly resonant with the atomic transition. The Doppler-free feature produced by saturation absorption of the counter-propagating pump beam further specifies the precise resonant frequency and reveals the natural linewidth of the transition.

Saturation absorption spectroscopy enables precise measurement of a given atomic transition while mitigating the effects of Doppler broadening.

2.3 Shelving Spectroscopy

Shelving spectroscopy is a technique used to enhance the detection of transitions with narrow linewidths by use of quantum state-selective detection. Quantum state-selection, in the context of atomic transitions, refers to the inability of an atom to be excited to two different states at the same time. This allows for the same sample of atoms to be interrogated beams at different frequencies, with each frequency resonant to a different atomic transition. Shelving spectroscopy is useful for measuring the precise resonant frequency for a transition with a relatively long lifetime. Atomic transitions with longer lifetimes are difficult to examine using a pure saturation absorption spectroscopy scheme. This is because transitions with longer lifetimes, and therefore narrower linewidths, have lower transition strengths. In other words, the probability that an atom will undergo a transition with a longer lifetime is lower than the probability that an atom will undergo a transition with a shorter lifetime. This leads to decreased levels of absorption that can be difficult to detect.

Atomic transitions with longer lifetimes also encourage higher-intensity interrogation of the sample. High-intensity beams, specifically the beams used as the pump in a saturation absorption scheme, can be increased for narrow, low-absorption transitions to increase absorption. This, however, may lead to power-broadening of the transition. Power-broadening occurs when the intensity of light interrogating a sample is so high that it significantly perturbs the atomic energy levels, causing an additional broadening of the transition.

Saturation absorption spectroscopy of transitions with narrow linewidths also leads to a decreased Doppler-free feature. The counter propagating pump and probe beams cancel out the effects of Doppler broadening at the precise frequency of the transition. However, given the decreased probability of absorption for narrow transitions, the contrast between the Doppler-broadened absorption and the Doppler-free lamb dip is diminished.

Shelving spectroscopy allows for the detection of narrow linewidth transitions while mitigating the effects of power-broadening and decreased absorption probability. Shelving spectroscopy

schemes involve an intermediate transition and a shelving transition. The first step in the shelving spectroscopy process is to excite atoms to a shelving state. The shelving state is a state characterized by its narrow linewidth and low transition probability that is difficult to examine directly in a saturation absorption scheme. Shelving states are often described as metastable due to their relatively long lifetimes. The long lifetime of a metastable state is typically due to the spin-forbidden nature of a transition from the excited state to a lower energy state.

The second step in the shelving spectroscopy process is to excite atoms that have decayed from the shelving state to an intermediate state. Because atoms must "wait" to decay from the metastable state to the ground state before they can be excited to the intermediate state, the absorption of a metastable transition can be measured as a decrease in absorption on the intermediate transition. Intermediate transitions are characterized by their short lifetimes, wide linewidths, and strong absorption. These characteristics allow for high-resolution measurements of the metastable transitions while not measuring the absorption of the metastable transition directly.

In the shelving spectroscopy scheme developed by Manai and colleagues, a thermal beam of strontium atoms is employed [13]. This thermal beam traverses two separate beams, each resonating with a distinct transition. The first beam resonates with the metastable transition. As illustrated in Figure 2.2, the intensity profile of the beam resonating with the metastable transition is considerably broader than that of the beam resonating with the intermediate transition. This effectively enhances the likelihood of an atom being excited to the metastable state without the need to increase the beam's intensity, thereby mitigating power broadening. Subsequently, the thermal beam of atoms passes through the beam resonating with the intermediate transition.

Atoms that have never been excited to the metastable state or those that have already decayed may then be excited to the intermediate transition. This excitation results in the absorption of photons from the beam, decreasing the intensity of light resonating with the intermediate transition as detected by a photodetector. However, since atoms excited to the metastable state and not yet decayed are incapable of being excited to the intermediate state, the absorption of light resonating with the intermediate transition is reduced in direct proportion to the number of atoms in the

metastable state. This method facilitates the measurement of light absorption resonating with the metastable state by monitoring the decrease in light absorption resonating with the intermediate transition.

Furthermore, this shelving spectroscopy scheme allows for a higher-resolution measurement of the metastable state than would be achievable by directly measuring the absorption of light resonating with the metastable transition. This is due to the higher probability of absorption to the intermediate transition compared to the metastable transition. Consequently, the transmission signal generated by the photodetector exhibits a more pronounced intensity difference by evaluating the absence of intermediate transition absorption rather than directly measuring the absorption of the metastable transition.

Owing to the enhanced signal strength provided by a shelving spectroscopy scheme, the Signal-to-Noise Ratio (SNR) for detecting the metastable transition is significantly improved. The SNR of an absorption profile is crucial for the development of an atomic clock. A higher SNR improves the quality of the error signal produced by a Lock-in Amplifier (LIA), which is employed to lock a laser to the resonance frequency.

Subsequent sections will investigate the combination of saturation absorption and shelving spectroscopy schemes. This fusion of techniques presents a potent tool for measuring metastable transitions. Saturation absorption spectroscopy mitigates Doppler broadening while shelving spectroscopy boosts the SNR for application in laser-locking schemes.

2.4 Strontium

The choice of atomic species is critical to the performance of atomic clocks. Strontium has emerged as an ideal candidate for atomic clocks with JILA developing a strontium clock with a world record instability with a deviation of only 1 second in roughly 5 billion years in 2014 [2][16] More recently, in 2022 the University of Wisconsin-Madison developed a strontium clock with the current world-record instability with a deviation of only 1 second in roughly 300 billion years [5]. Strontium is a superb candidate for atomic clock development due to its simple valence electron

Figure 2.2: Shelving spectroscopy of a thermal beam of strontium atoms. The thermal beam first passes through a retro-reflected beam resonant with the metastable transition. The thermal beam then passes through a beam resonant with an intermediate transition. The absorption profile of the intermediate transition is then measured using a photodetector [13].

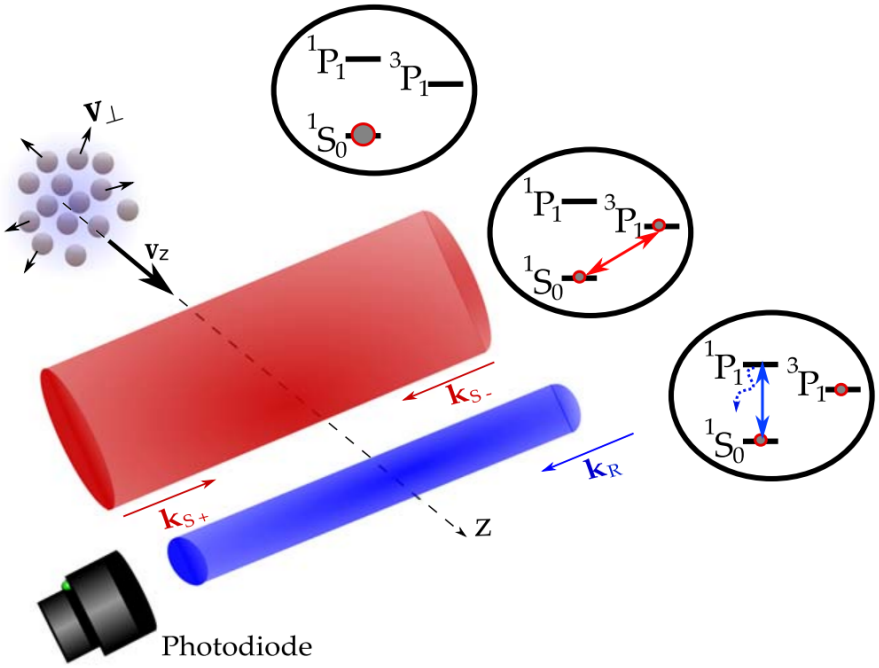

structure, its capacity for both broad and narrow linewidth optical transitions, its monatomic structure in its gaseous state, and its sufficient vapor pressure at low oven temperatures.

The electron structure of strontium is characterized by a simple valence electron configuration. Its outermost shell consists of only two valence electrons. This is advantageous for atomic clocks as it results in a reduced number of hyperfine interactions that could otherwise broaden the linewidth of transitions, thus compromising the clock's accuracy. Furthermore, the simple electronic structure makes strontium more amenable to theoretical modeling and analysis.

Strontium possesses both spin-permitted and spin-forbidden optical transitions. This allows for shelving spectroscopy schemes that utilize the long lifetime spin-forbidden transitions with an improved signal-to-noise ratio by utilizing the short lifetime of spin-permitted transitions. Spin-forbidden transitions, which exhibit extremely narrow linewidths, are particularly useful for ultra-high precision atomic clocks. The narrow linewidth minimizes frequency instability and enables the clock to maintain accuracy over long periods of time.

In its gaseous state, strontium exists as a monatomic species. This monatomic structure eliminates the need to account for molecular interactions which can introduce additional uncertainty. Additionally, the absence of molecular interactions simplifies the interpretation of the absorption signal, contributing to the overall accuracy and stability of strontium-based atomic clocks.

Strontium exhibits favorable vapor pressure at relatively low oven temperatures between 200°C and 550°C [1][19]. This property simplifies the design of strontium-based clocks as it minimizes potential thermal gradients and associated systematic errors. Furthermore, the low operating temperature prolongs the lifetime of the atomic clock apparatus by reducing the reaction of strontium atoms with its silica enclosure.

Chapter 3

Experimental Design

3.1 Micro-fabricated Vapor Cells

The National Institute of Standards and Technology (NIST) has been at the forefront of research into micro-fabricated vapor cells, which are central to the development of Chip-Scale Atomic Clocks (CSACs) [9][8][10]. CSACs allow for remarkable precision of atomic clocks in a miniaturized, low-power package. Early work demonstrated the feasibility of chip-scale atomic devices, which laid the groundwork for subsequent innovations in miniaturized atomic clocks [8][10].

The vapor cell fabrication process involves depositing thin layers of alkali or alkaline metal and a buffer gas within a hermetically sealed silica cavity [12][21]. The micro-fabricated vapor cells have dimensions on the order of millimeters, significantly smaller than conventional vapor cells, which are typically several centimeters in size [12][15]. The size of these cells ensures their compatibility with micro-electromechanical systems (MEMS) technology.

Micro-fabricated vapor cells exhibit similar performance to their larger counterparts in terms of optical absorption properties and alkali metal vapor densities [8]. Furthermore, the micro-fabricated vapor cells show no significant change in performance when operated at elevated temperatures, indicating their potential for use with atomic species that require oven temperatures for adequate vapor pressure [8].

The research design outlined in this paper demonstrates the feasibility of micro-fabricated silica vapor cells containing strontium for use in CSACs. Although the size of this experimental design is on the order of 10 square meters, all electronic and optical components can be miniaturized

to chip scale.

3.2 Vacuum and Oven

In the experimental design presented in this paper, the vapor cell is positioned within a ceramic oven. This oven is heated by a thin wire threaded through each hole in an alternating pattern. A potential difference applied across the wire generates heat. Figure 3.2 below depicts the ceramic oven and its associated wire.

The ceramic oven is subsequently positioned within a stainless steel sleeve, which serves as a holder for both a temperature probe and wire connections to an external voltage source. After this assembly, the oven and sleeve are carefully placed inside a vacuum chamber. Figure 3.3 provides a image of the arrangement.

The vacuum chamber is hermetically sealed using a lid (not shown). The internal pressure of the chamber is reduced to approximately $1 * 10^{-}4$ mbar, effectively minimizing thermal conduction losses to the surrounding atmosphere. A potential difference ranging from 20 to 25 volts is applied across the wire, heating the vapor cell to temperatures exceeding 200°C. Upon reaching temperatures above this threshold, the vapor pressure within the cell rises to at least $3.5 * 10^{-}8$ mBar [19]. This vapor pressure allows for sufficient absorption and precise measurement of atomic transitions.

3.3 Atomic Transitions of Strontium

In this experiment, the atomic transitions of interest are located at wavelengths of 461 nm and 689 nm. These wavelengths are calculated by converting the transition energy to light frequency, then converting to wavelength in a medium with an index of refraction close to 1, and subsequently rounding to the nearest nanometer. The 689 nm transition is the spin-forbidden transition from the $^1S_0$ ground state to the $^3P_1$ metastable state, while the 461 nm transition is the permitted transition from the $^1S_0$ to the $^1P_1$ intermediate state. The 689 nm transition is characterized by its relatively long lifetime ($\tau = 21$ μs) and narrow linewidth ($\Gamma = 2\pi \times 7.6$ kHz), in contrast to the shorter lifetime ($\tau = 5$ ns) and broader linewidth ($\Gamma = 2\pi \times 32$ MHz) of the 461 nm transition. A

Figure 3.1: Scale of a Micro-fabricated Vapor Cell (Credit: Dr. Matthew Hummon) [17]

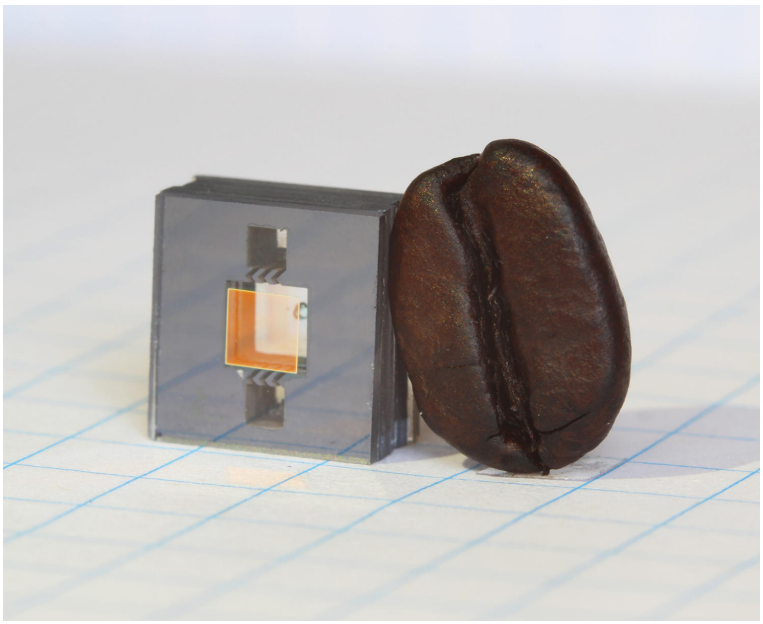

Figure 3.2: Vapor Cell Oven. (a) Displays the holes for the heating wire and the larger porthole allowing for laser interrogation of the vapor cell. (b) Exhibits the chamber for the vapor cell.

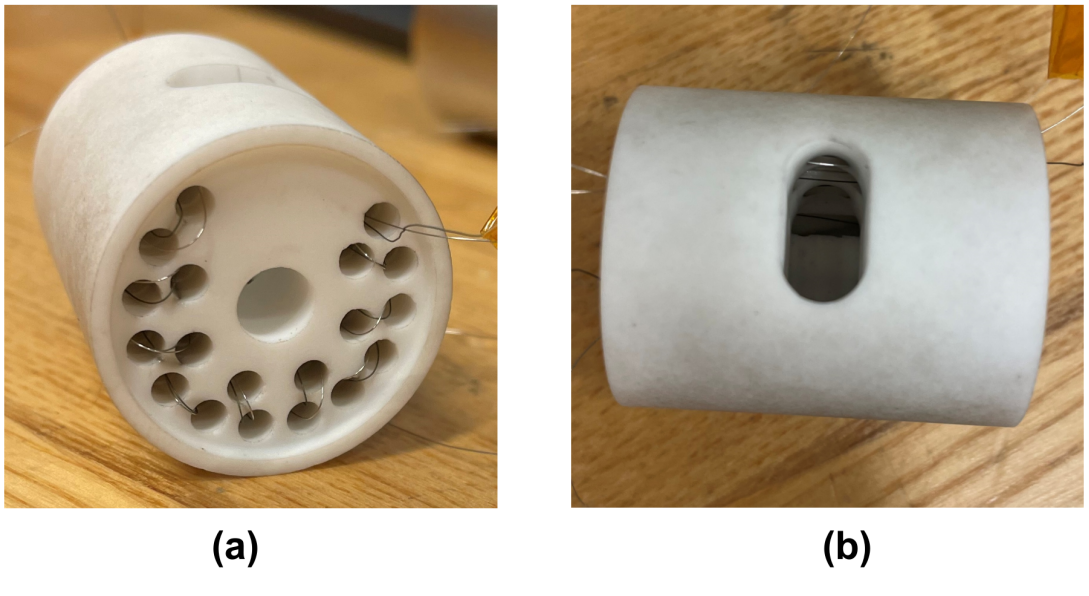

Figure 3.3: Vacuum Chamber and Oven. (a) The ceramic oven and stainless steel sleeve are situated inside the vacuum chamber, with the temperature probe inserted through the top of the sleeve and extending into the vapor cell groove. (b) The two ceramic tubes projecting horizontally from the sleeve enable connections to an external voltage source.

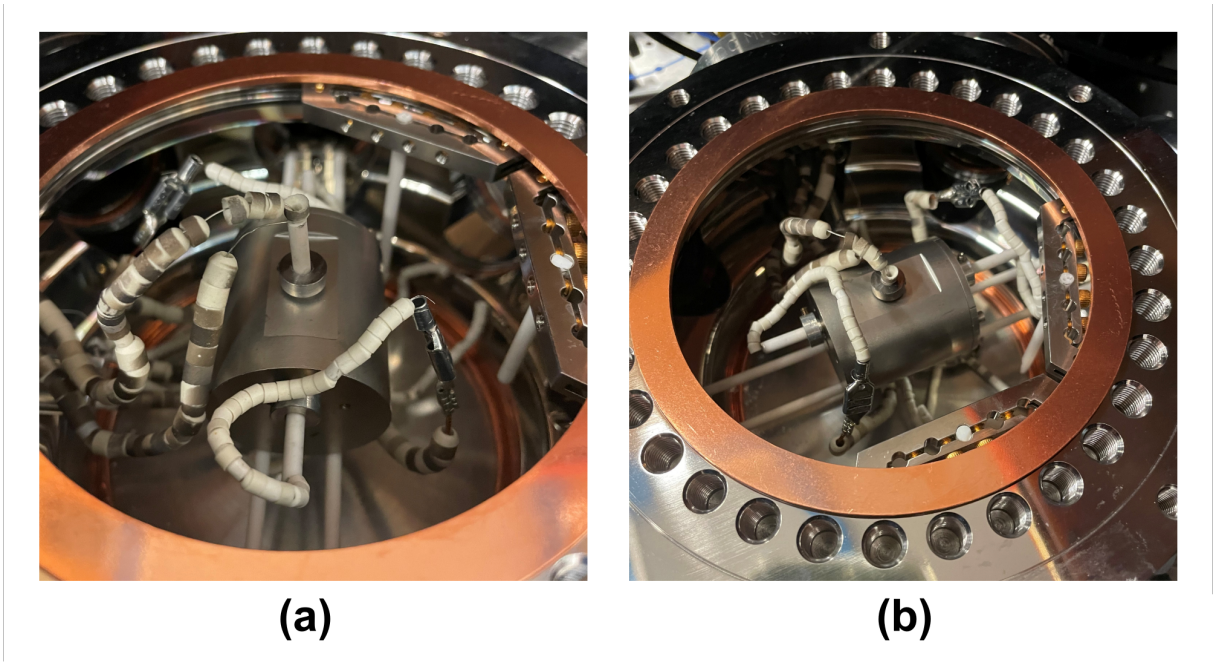

simplified atomic transition structure of strontium can be observed in Figure 3.4.

For the atomic clock, the goal is to "lock" a laser to the 689 nm transition. The narrow linewidth of the 689 nm transition signifies that only light within a 7.6 kHz deviation from the transition frequency, which is approximately 435 THz, will be detected. This corresponds to a maximum fractional frequency deviation of approximately $2 \times 10^{-}11$ (1). In contrast, utilizing the 461 nm transition would yield a maximum fractional deviation of approximately $6 \times 10^{-}8$ (1), resulting in a precision that is about 3,300 times worse (2). The diminished fractional deviation of a laser in resonance with the 689 nm transition leads to enhanced performance when compared to a clock relying on a laser in resonance with the 461 nm transition.

Atomic transition linewidths can be compared for their use in a clock by calculating their respective Minimal Clock Precisions (MCPs). The MCP is a measure of the minimum amount of time it would take for a clock utilizing a given transition to deviate by 1 second. See Appendix A Equation 3 for the MCP equation. The MCP for the 461 nm transition is approximately 0.64 years. In other words, a clock utilizing a laser locked to the 461 nm transition will deviate by 1 second in a minimum of 0.64 years if the frequency of the laser deviates from the resonance frequency by the linewidth of the transition. Conversely, the MCP for the 689 nm transition is approximately 1815.44 years, in other words, the precision of the 689 nm transition is at least 2836 times better than the 461 nm transition. It is important to note that the exact precision of a clock utilizing each transition is far greater than their respective MCPs. A lattice clock utilizing the $^1S_0$ to $^3P_0$ strontium transition, which has a linewidth $\Gamma = 2\pi \times 1$ mHz achieved an estimated deviation of 1 second in 5 billion years [2].

3.4 Shelving Spectroscopy of a Vapor Cell

In this experiment, the shelving spectroscopy scheme employs the 461 nm transition as the intermediate state and the 689 nm transition as the metastable state. In contrast to the shelving scheme utilizing a thermal beam shown in Figure 2.2, the shelving scheme for this experiment interrogates a micro-fabricated vapor cell containing strontium with coaligned beams of 461 nm and

Figure 3.4: Simplified Atomic Transition Structure of Strontium. The 461 nm intermediate transition is denoted in blue. The 689 nm metastable transition is denoted in red.

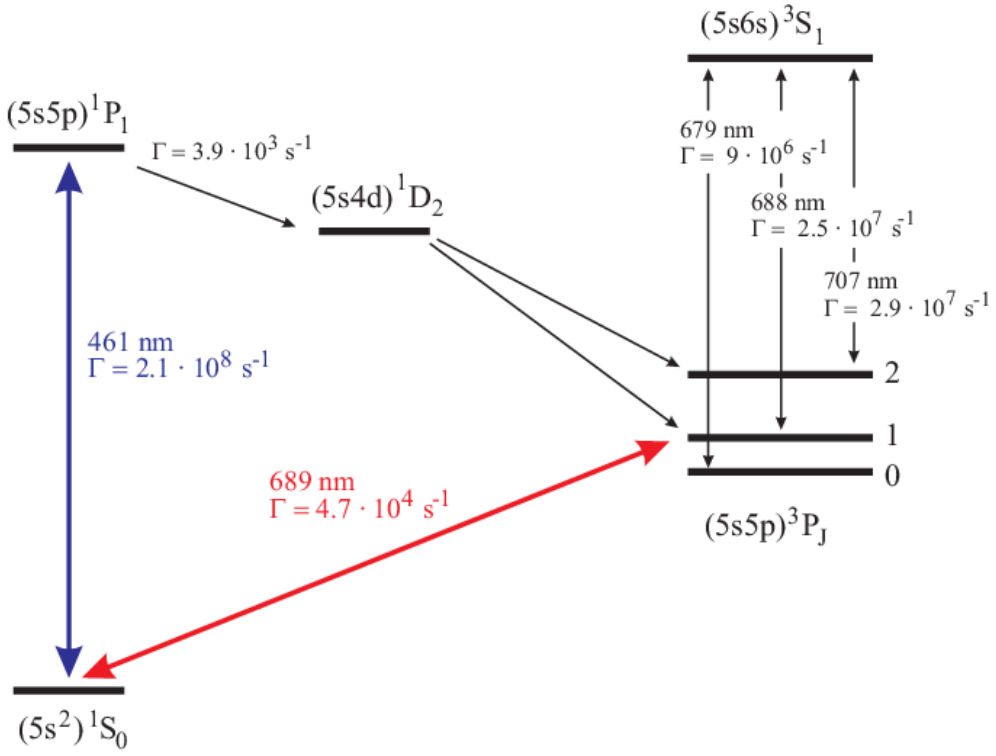

689 nm light. Figure 3.5 shows the shelving arrangement that inspired the arrangement ultimately used in this paper [13].

The radius of the intensity profile for the 689 nm light is designed to interrogate the largest feasible cross-section of the vapor cell. In the experiment outlined in this paper, the intensity profile is limited by the diameter of the porthole shown in Figure 3.2. The radius of the porthole is approximately 2 mm.

3.5 Optical Arrangement

The optical arrangement for the experiment outlined in this paper is analogous to the arrangement shown in Figure 3.5.

Analogous to Figure 3.5, in Figure 3.6, the 689 nm laser light is retro-reflected back across the sample to reduce Doppler broadening on the 689 nm transition. Furthermore, a saturation absorption scheme for the 461 nm transition to reduce Doppler broadening. The saturation absorption scheme is accomplished by dividing the light into a pump and a probe beam using a polarizing beam-splitting cube (PBS).

The polarization of the 461 nm light is adjusted prior to the PBS with the aid of a Half-Wave Plate (HWP) to ensure that the pump beam's intensity is approximately 100 times greater than that of the probe beam. Light from the probe beam traverses an Acousto-Optic Modulator (AOM) without undergoing frequency modulation and is subsequently reflected back through the strontium sample. When AOM #1 is activated, a first-order beam of 461 nm light passes through the iris and is reflected through the strontium sample. The inclusion of the AOM allows for the selective activation and deactivation of Doppler-free spectroscopy as needed.

In this experiment, the 461 nm laser is simultaneously scanned and modulated at frequencies of 5 Hz and 20 MHz, respectively. The laser undergoes a scan at a rate of 5 Hz, because the laser will not be resonant with the transition frequency prior to being locked. The 5 Hz scan is a current scan performed directly on the 461 nm laser, sweeping its frequency over a range of approximately 10 GHz. Given that the 461 nm laser can be manually tuned to within 0.01 THz of the resonant

Figure 3.5: Simplified Shelving Arrangement [13] The diagram depicts a shelving spectroscopy arrangement for the 689 nm intercombination line that can be used for a micro-fabricated vapor cell.

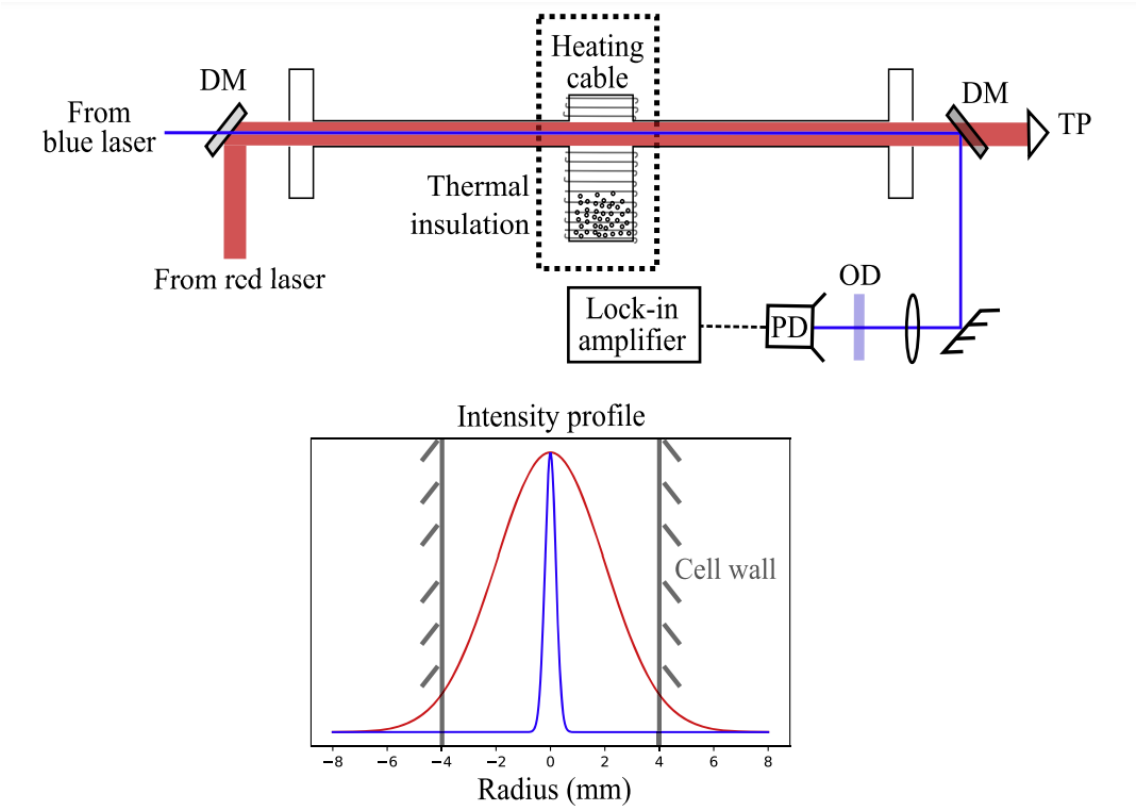

Figure 3.6: Optical Arrangement for the Experiment.
M = Mirror; Iso = Optical Isolator; HWP = Half Wave Plate; FP = Fiber Port; FS/C = Fiber Splitter/Coupler; PBS = Polarizing Beam Splitter; Exp = Optical Expander; AOM = Acousto-Optic Modulator; L = Lens; QWP = Quarter Wave Plate; DM = Dichromatic Mirror; BS = Beam Splitter; PD = Photodiode; A = Optical Attenuator

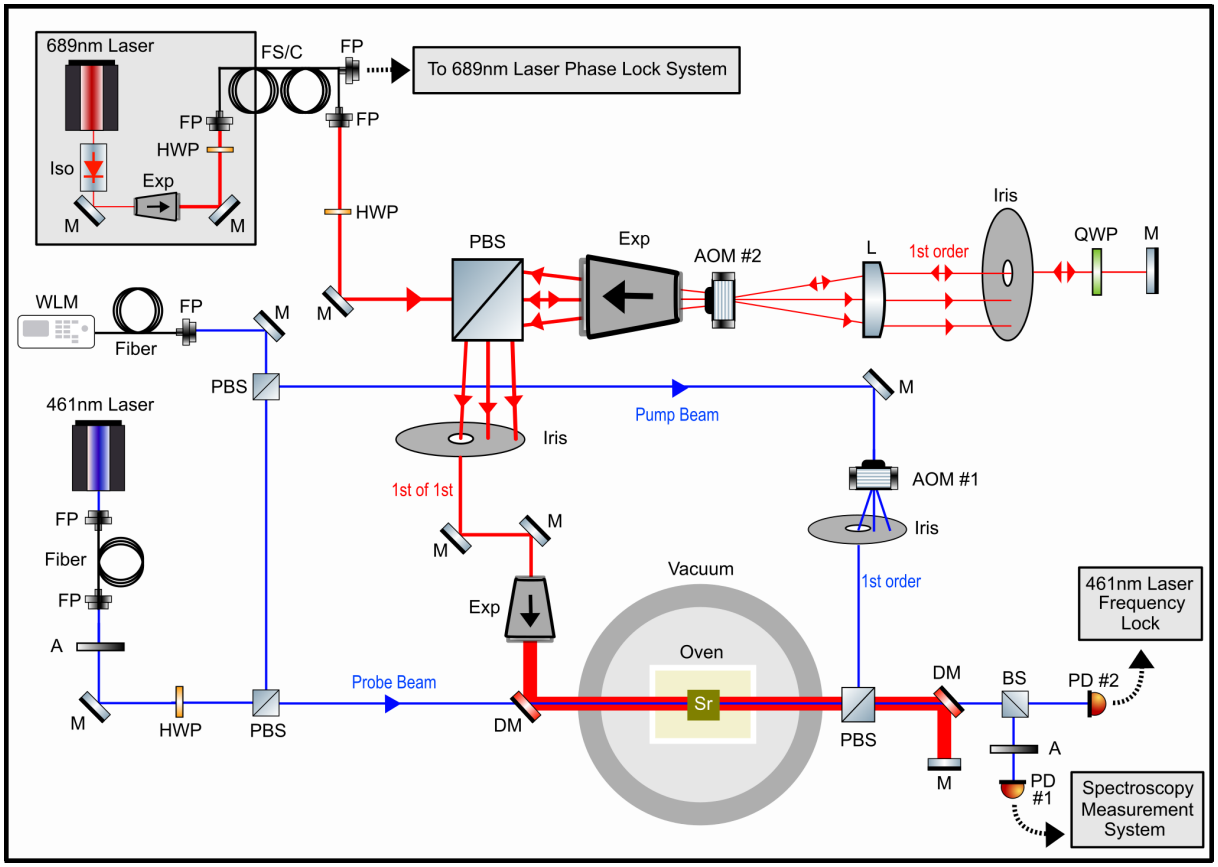

frequency, we can ascertain that the initial frequency of the laser deviates by no more than 10 GHz from the transition frequency. The yellow curve in Figure 3.7 illustrates the photodiode output corresponding to such a sweep.

The output of a photodiode is determined by the intensity of light impinging on the diode. Since saturation absorption spectroscopy assesses the absorption of a transition based on the reduction in light transmission through the sample, the yellow curve in Figure 3.7 above reaches its maximum when there is minimal absorption, and thus, maximal transmission of light at the 461 nm transition. Conversely, the yellow curve is at its minimum when there is maximal absorption and minimal transmission of light. This indicates that the frequency of light emitted by the 461 nm laser precisely matches the 1S0 to 1P1 transition of strontium at the exact frequency that induces minimal transmission on the yellow curve. Figure 3.7 also exhibits a minor Doppler-free feature observable near the point of minimum transmission. Figure 3.8 presents the same image as Figure 3.7, but with a closer view to effectively highlight the Doppler-free feature.

In Figure 3.8, the Doppler-free feature is discernible as a small, narrow peak near the point of minimal transmission. The seemingly noisy region between the Doppler-free peak and the yellow transmission curve is, in fact, not noise. Rather, this "haziness" results from the transistor-transistor logic (TTL) modulation of AOM #1. The Doppler-free feature is crucial for a precise frequency lock of the 461 nm laser to the $^1S_0$-$^1P_1$ transition. The frequency lock for the 461 nm laser will be elaborated in future sections.

Figure 3.7: The 5Hz scan spans a frequency range of approximately 10 GHz. The yellow curve is the absorption profile of the 461 nm transition. Each local minimum on the yellow curve indicates near-maximum absorption. The linewidth of each absorption "dip" is broadened beyond the natural linewidth of the transition. The pink curve is the scan signal sent to the laser controller for the 461 nm laser. The x-axis measures time, with each long vertical tick on the x-axis denoting 50 ms. The y-axis measures voltage.

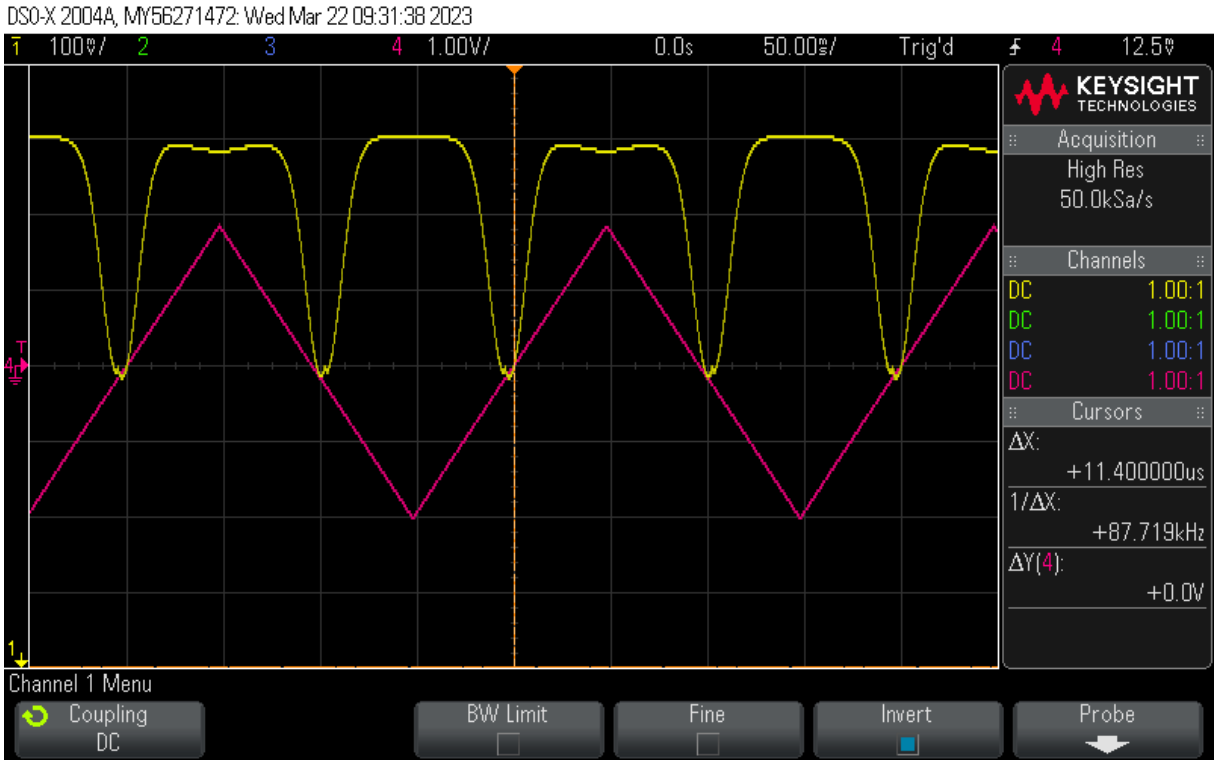

Figure 3.8: The Doppler-free feature is generated via activation of the probe beam by AOM #1 in Figure 3.6. The x-axis represents time, and the y-axis measures voltage.

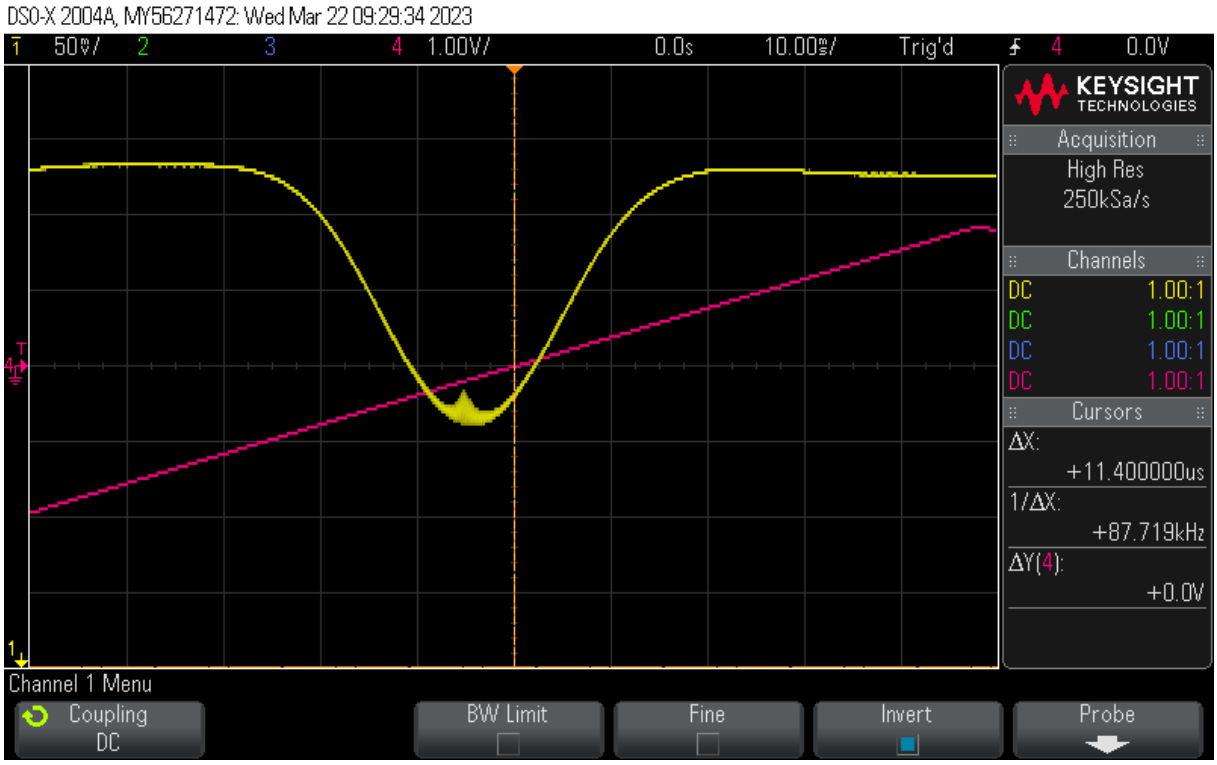

Chapter 4

Frequency Lock

Since we are employing a shelving spectroscopy scheme for our clock, the precision of our clock will largely rely on the quality of the lock for the intermediate transition. The more precisely we can lock the 461 nm laser to the $^1S_0$-$^1P_1$ transition, the higher quality data we can collect on the absorption of the 689 nm laser light by the $^1S_0$-$^3P_1$ transition.

4.1 Lock-in Amplifier

A conventional frequency lock configuration utilizes a single lock-in amplifier (LIA). An LIA is comprised of an input signal, a reference signal, a mixer, a low-pass filter, and an amplifier. The LIA mixes the input signal with the reference signal, aiming to measure the difference between the component of the input signal that is closest in frequency to the reference signal and the reference signal. In our experiment, the intensity modulation of the laser light is detected by the photodiode. The intensity modulation results from the frequency modulation by the reference signal. This intensity modulation is referred to as the dither signal. This dither signal, which varies based on the saturated absorption of the strontium sample, is what the LIA measures against the reference. To provide a concrete example, let's consider an input with a dither signal 4.1 and a reference signal 4.2.

$$V_d = A\sin(2\pi f_d t + \phi_d) \tag{4.1}$$

$$V_r = B\sin(2\pi f_r t + \phi_r) \tag{4.2}$$

In this case, f_d and ϕ_d are the dither frequency and phase, while f_r and ϕ_r denote the dither frequency and phase. The values A and B are the amplitudes of the dither and reference signals respectively, with units of potential difference. Assuming that V_d and V_r are synchronized to be in phase with each other, we can proceed assuming $\phi_d = \phi_r = 0$. When the LIA receives both the dither and reference signals, the mixer within the LIA multiplies the dither and reference signals, producing a mixed signal 4.3.

$$V_{mixed} = AB\sin(2\pi f_d t) \times \sin(2\pi f_r t) \tag{4.3}$$

Subsequently, this equation can be simplified to the following sum 4.4

$$V_{mixed} = \frac{AB}{2}[\cos(2\pi[f_d - f_r]t) - cos(2\pi[f_d + f_r]t)] \tag{4.4}$$

When the laser's frequency is resonant with the atomic transition frequency, the dither signal's frequency is twice the frequency of the reference, i.e. $f_d = 2f_r$. This is because one dither cycle, or one 20 MHz frequency cycle on the laser, will approach maximum absorption halfway through the reference cycle and then recede from maximum absorption for the second half of the reference cycle. This effectively doubles the frequency of the dither signal measured by the photodiode, while halving its amplitude. So, when the laser light is resonant with the transition, the dither signal's frequency is $2f_r$, resulting in a dither signal described by the following Equation 4.5.

$$V_{in} = A\sin(4\pi f_r t) \tag{4.5}$$

By substituting Equation 4.5 for the dither signal in Equation 4.4 for the mixed signal, we obtain Equation 4.6 for the mixed signal, where $X_1 = X_2 = 1$ are the new individual amplitudes for each term, and $\frac{AB}{2}$ is the amplitude of the whole mixed signal.

$$\text{Low-passed} \quad V_{mixed} = \frac{AB}{2}[X_1 \cos(2\pi f_r t) - X_2 \cos(6\pi f_r t)] \tag{4.6}$$

The amplitude of each component of the mixed signal is then attenuated by a low-pass filter, which significantly reduces the amplitude of each periodic signal, effectively yielding a DC signal at 0V. This can be seen in the following calculation of Equation 4.9.

$$\begin{aligned} \text{Low-passed} \quad V_{mixed} &= \lim_{X_1, X_2 \to 0} \frac{AB}{2}[X_1 \cos(2\pi f_r t) - X_2 \cos(6\pi f_r t)] && (4.7) \\ &= \frac{AB}{2}[0 \cos(2\pi f_r t) - 0 \cos(6\pi f_r t)] && (4.8) \\ &= 0 && (4.9) \end{aligned}$$

Conversely, when the laser frequency is not resonant with the atomic transition, one dither cycle has a frequency less than $2f_r$. A dither cycle, when the laser is not resonant with the transition, has a minimum frequency of f_r. The resulting output has a non-zero DC component. For the purpose of the following sequence of equations, the dither frequency can be assumed to be f_r without loss of generality. Thus, assuming a minimum dither frequency of f_r results in Equation 4.10 for the dither signal.

$$V_in = A \sin(2\pi f_r t) \tag{4.10}$$

Multiplying this non-resonant dither signal with the reference signal, Equation 4.2, results in a mixed signal containing a DC component. The subsequent mixed signal, Equation 4.15, is computed using the sequence of equations outlined below.

$$\begin{aligned} V_{mixed} &= V_r \times V_d && (4.11) \\ &= A \sin(2\pi f_r t) \times B \sin(2\pi f_r t) && (4.12) \\ &= \frac{AB}{2}[\cos(2\pi[f_r - f_r]t) - \cos(2\pi[f_r + f_r]t)] && (4.13) \end{aligned}$$

$$= \frac{AB}{2}[\cos(0) - \cos(4\pi f_r t)] \tag{4.14}$$

$$V_{mixed} = \frac{AB}{2}[1 - \cos(4\pi f_r t)] \tag{4.15}$$

The amplitude of each term in the mixed signal is attenuated by a low-pass filter. This causes the amplitude of each periodic signal to approach zero. Taking the limit of the amplitude analogous to the limit in Equation 4.9 results in Equation 4.16.

$$V_{mixed} = \frac{AB}{2} \tag{4.16}$$

This indicates that when the laser's frequency is not resonant with an atomic transition, a direct current (DC) signal, referred to as the error signal, is generated. A comparison between resonant and non-resonant dither signals can be observed in Figure 4.1.

The DC error signal provides two crucial pieces of information. Firstly, it indicates whether the frequency of our laser is higher or lower than the resonant frequency. Secondly, if the dither frequency is not equal to the reference frequency, the error signal reveals the proximity of the laser frequency to the resonant frequency. The relationship between the error signal and the laser's angular frequency is visualized in Figure 4.2

This error signal is sent to a Proportional-Integral-Derivative (PID) controller. The PID controller then adjusts the current applied to the laser to achieve an error signal of 0 V. As shown in Equation 4.9, an error signal of 0 V indicates that the laser is resonant with its transition. This continual adjustment of the laser by the PID controller is what "locks" the laser to the resonance frequency.

4.2 Tandem Lock-in Amplifiers

For the frequency lock of the 461 nm laser, we will be using a tandem LIA system. The tandem LIA system consists of two Lock-in amplifiers, with the first LIA constructed from in-house components to facilitate a 20 MHz reference frequency, which is too high for most commercial LIAs. Figure 4.3 shows the tandem LIA system used for the frequency lock.

Figure 4.1: Relationship between the Dither Frequency and Resonance Frequency. In this figure, ω_d is the angular frequency of the non-resonant dither signal, $2\omega_d$ is the angular frequency of the resonant dither signal, and ω_0 is the resonance angular frequency. [7]

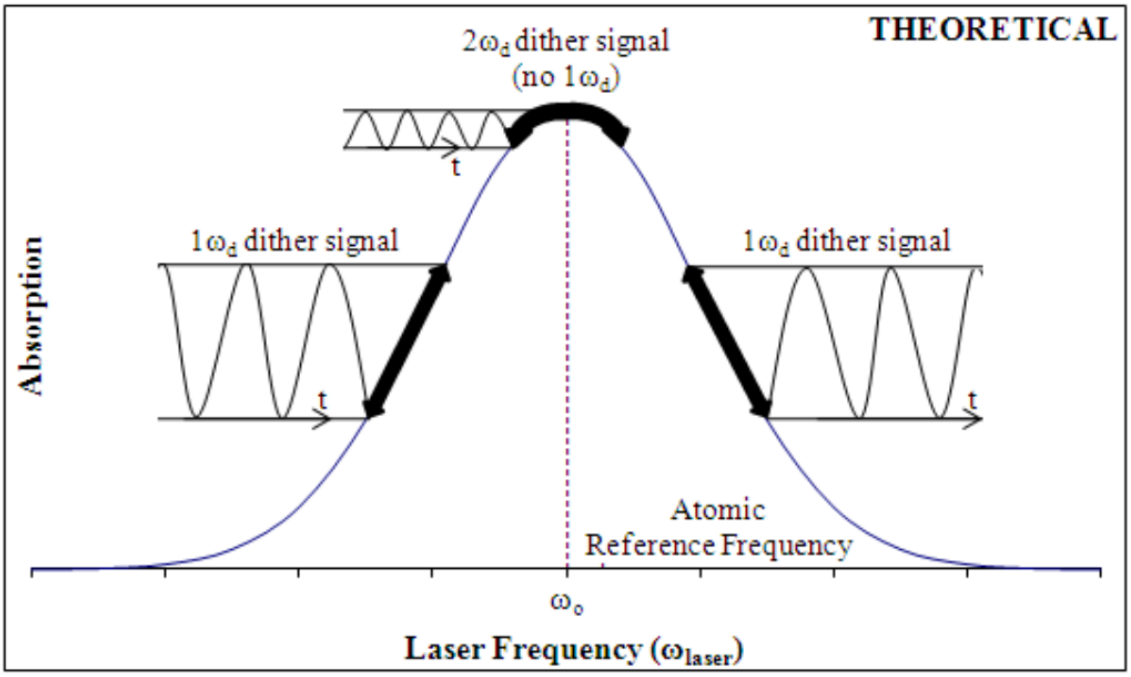

Figure 4.2: Error Signal and Resonance Frequency Relationship. The relationship between the laser frequency and the error signal. A negative error signal indicates that the laser frequency is higher than the resonant frequency, while a positive error signal indicates that the laser frequency is lower than the resonant frequency. [7]

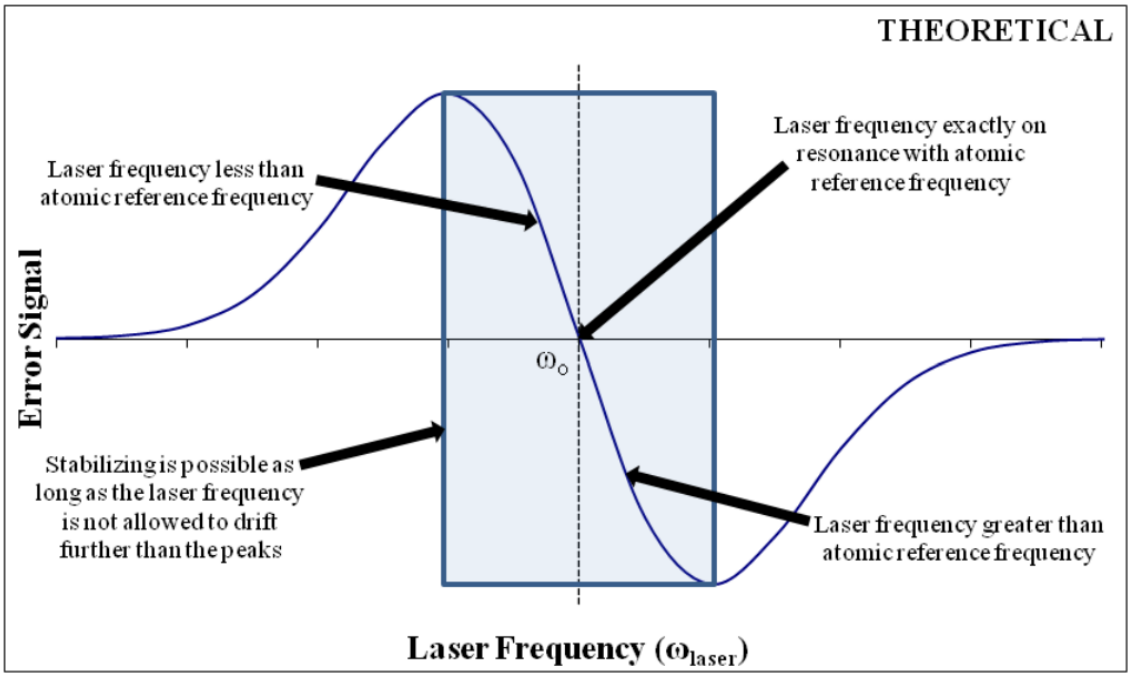

Figure 4.3: Tandem Lock-in Amplifier System. The first LIA is constructed to facilitate a 20 MHz reference frequency, producing an error signal with DC and AC components. The second LIA, a Stanford Research Systems Model 830, removes the remaining AC component, thus producing a purely DC error signal that is utilized for the frequency lock.

PD = Photodiode or Photodetector; Amp = Electronic Amplifier; FG = Function Generator; LP = Low Pass Filter; LIA = Lock-in Amplifier; Osc = Oscilloscope; PID = PID controller, or servo; LC = Laser controller.

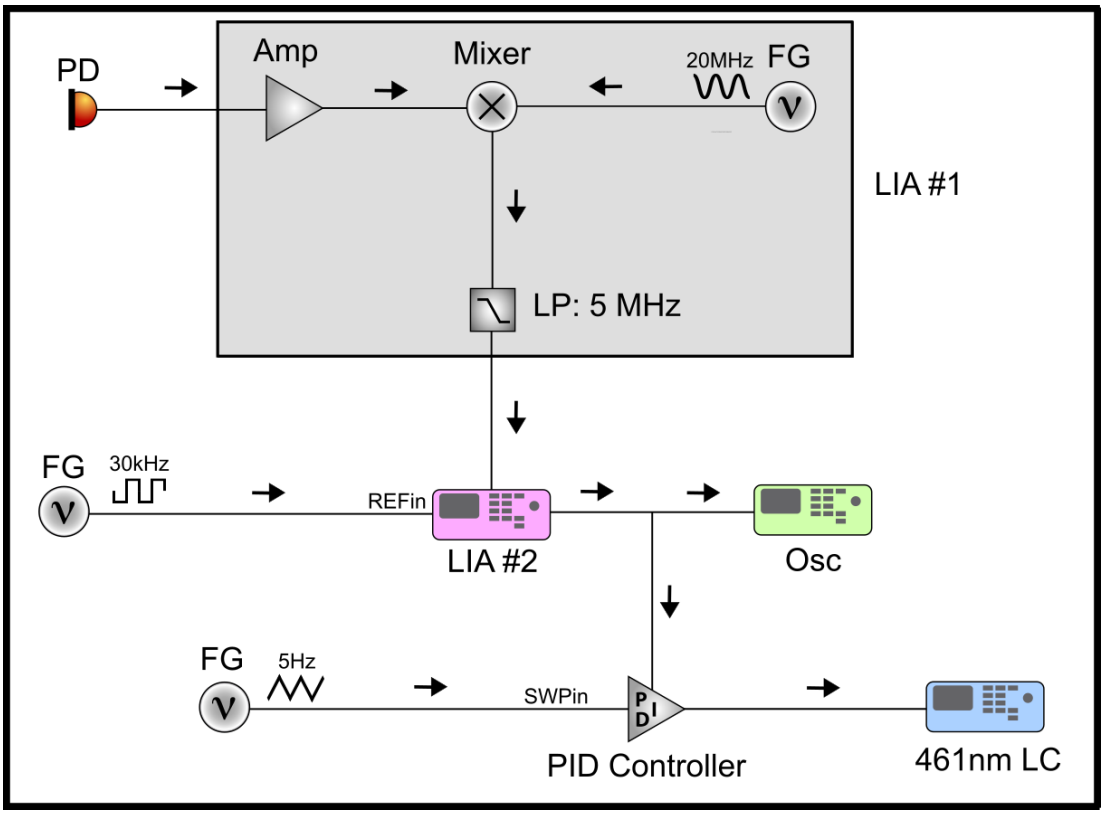

The purpose of employing a tandem LIA system is to improve the precision of the frequency lock. Using a single LIA would allow us to lock the 461 nm laser using the near-maximum, local minimum feature of the photodetector output. However, since the absorption profile is Doppler broadened, the quality of a lock based only on this signal will be imprecise. High precision is necessary for adequate measurement and subsequent lock of the 689 nm laser to the metastable transition.

The first LIA receives the unprocessed absorption signal from the photodiode shown in Figure 3.7. This LIA generates an error signal using the local minimum component of the absorption profile. The 20 MHz reference signal for the first LIA is also the signal used to create the dither signal on the 461 nm laser. Inserting 20MHz for the frequency of the reference, f_r, in Equation 4.4 for the mixed signal, we get Equation 4.17.

$$V_{mixed} = \frac{AB}{2}[\cos(2\pi[f_d - 20MHz]t) - \cos(2\pi[f_d + 20MHz]t)] \tag{4.17}$$

If the frequency of the 461 nm laser is resonant with near-resonance, maximum absorption frequency, then the dither frequency is equivalent to twice the reference frequency, i.e. $f_d = 40$ MHz.

$$V_{mixed} = \frac{AB}{2}[\cos(2\pi \times 20MHz \times t) - \cos(2\pi \times 60MHz \times t)] \tag{4.18}$$

The amplitude of each of the AC components of V_{mixed} is attenuated by the 5 MHz low pass filter. Analogous to the sequence of equations 4.9, a 0V DC output is produced by the first LIA, indicating resonance with the near-resonance, maximum absorption frequency for the 461 nm transition. Conversely, If the frequency of the 461 nm laser is not resonant with the maximum absorption frequency, then the dither frequency on the input is equivalent to the reference frequency. This results in Equation 4.19 for the non-resonant mixed signal.

$$V_{mixed} = \frac{AB}{2}[\cos(2\pi[0MHz]t) - \cos(2\pi[40MHz]t)] \tag{4.19}$$

Further simplifying produces Equation 4.20.

Figure 4.4: Modulation Diagram AOM #1. AOM #1 operates at 80 MHz, while its drive frequency undergoes TTL modulation at 30 kHz.

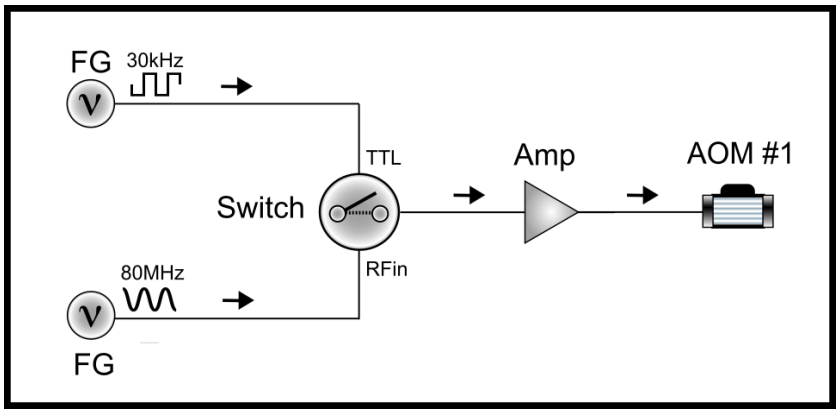

$$V_{mixed} = \frac{AB}{2}[1 - \cos(2\pi[40MHz]t)] \tag{4.20}$$

The 5MHz low pass filter attenuates the 40MHz component of the mixed signal. This results in a DC output component equivalent to Equation 4.21.

$$V_{mixed} = \frac{AB}{2} \tag{4.21}$$

The second LIA employs a 30 kHz AC component to generate an error signal exhibiting the Doppler-free characteristic. This feature is modulated at 30 kHz by a TTL switch controlling the drive frequency of AOM #1. The resulting TTL modulation gives rise to the observed "haziness" in the Doppler-free feature depicted in Figure 3.8. Figure 4.4 illustrates the configuration enabling the AOM modulation.

For the lock's precision, it is crucial that the first AOM disregards the Doppler-free dither while the second AOM processes it. This arrangement allows the first AOM to generate a DC error signal based on the Doppler-broadened absorption profile, and the second AOM to produce a DC error signal founded on the narrow Doppler-free feature. The mixer selected for the first LIA is a Mini-Circuits ZFM-3-5+ mixer, which boasts a mixing range between 40 kHz and 300 MHz. This permits the Doppler-free feature to be dithered at 30 kHz without being mixed with the 20 MHz

reference in the first LIA. The 30 kHz dither is then utilized by the second LIA to generate an error signal solely relying on the Doppler-free characteristic. Figure 4.5 presents the modulated drive signal for AOM #1.

The rationale behind using a TTL switch for modulating the drive frequency, rather than direct modulation, lies in the importance of maintaining coherence between the pump and probe beam frequencies. Coherence between the two beams ensures that the Doppler-free feature materializes at the precise resonance frequency for the ^{1}S0-^{1}P1 transition.

The Doppler-free dither frequency undergoes processing by the second AOM, analogous to the first AOM's handling of the 20 MHz frequency modulation. This generates a pure DC error signal, which is the sum of the DC components of the error signal produced by each AOM. This error signal is then transmitted to a PID controller. This PID controller is what enables the initial 5 Hz sweep of the 461 nm laser. Utilizing the error signal, the PID controller determines the direction and extent of deviation of the 461 nm laser from the resonance frequency. If the error signal is equivalent to 0V, the PID makes no adjustment to the current of the 461 nm laser. However, if the error signal is non-zero, the PID controller modifies the current applied to the 461 nm laser in a manner that reduces the error signal's magnitude. This continuous adjustment process by the PID controller constitutes the "lock" of the 461 nm laser to the resonance frequency for the ^{1}S0-^{1}P1 transition.

Nonetheless, the PID cannot instantaneously lock the 461 nm laser while the 5 Hz sweep spans an optical frequency range on the order of 10 GHz. This is because the error signal's magnitude is dominated by the scan, rather than the 20 MHz and 30 kHz dither frequencies. Consequently, to lock the 461 nm laser, the span must be manually reduced so that the optical bandwidth of the scan sufficiently decreases, allowing the error signal's magnitude to be dominated by each dither frequency.

In order to facilitate a small enough scan of the 461 nm laser to enable frequency lock, two steps are undertaken. Firstly, the Doppler-free feature is adjusted to be as close as possible to the center of the scan. This is visually indicated by the photodetector output in Figure 3.7, where

Figure 4.5: The blue curve is the TTL-modulated drive frequency transmitted to AOM #1, as depicted in Figure 4.4. The drive frequency is absent for half of the TTL cycle, effectively switching the AOM on and off at a rate of 30 kHz. This process enables the generation of a dither frequency on the Doppler-free feature while preserving coherence between the probe and pump beams.

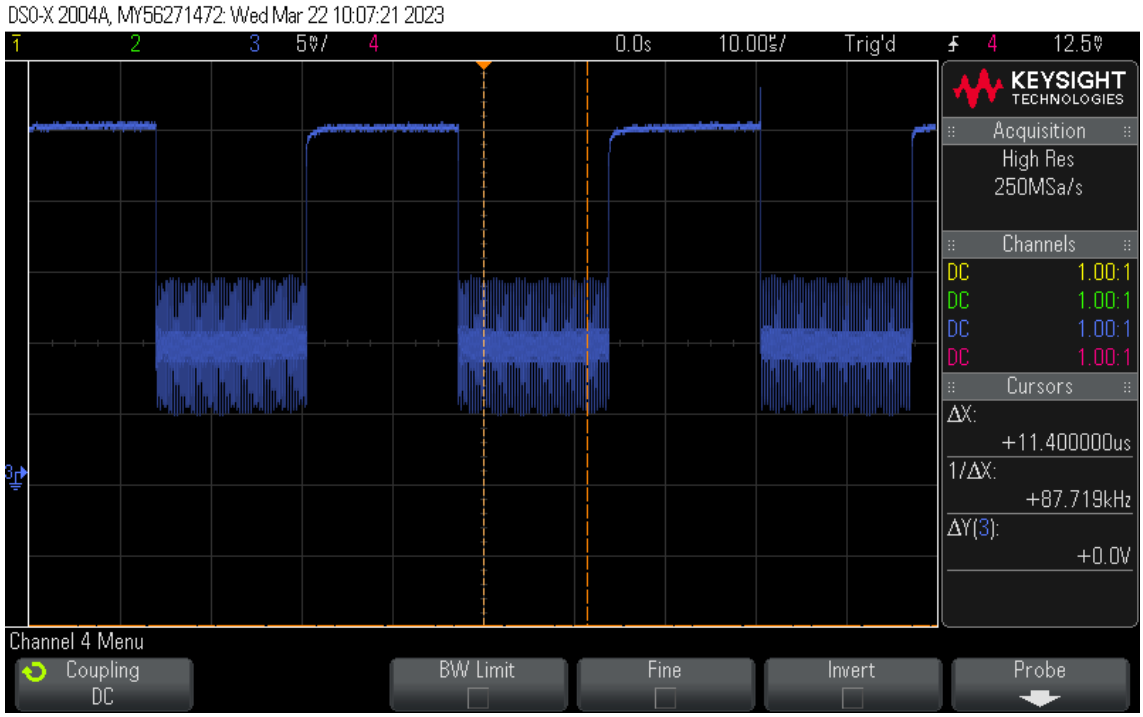

the Doppler-free feature is centered on the triangular scan function's zero-crossing. The span is then incrementally decreased until it reaches the minimum value at which the Doppler-free feature remains visible, signifying that the laser is still momentarily resonant with the ^{1}S0-^{1}P1 transition during its scan. Upon enabling the PID lock, the PID controller's electronics maintain the frequency lock by utilizing the tandem LIA system error signal. The gradual reduction of the 461 nm laser scan can be observed in Figure 4.6.

Figure 4.6: Reduction in Bandwidth of 5 Hz Scan. Subplot (a) shows the initial absorption profile prior to scan reduction. Subplot (d) shows the final absorption profile after the scan has been maximally reduced such that the Doppler-free feature is still present. The pink triangle wave depicts the initial scan signal. The scan signal does not decrease in each subplot because the reduction in the scan is handled directly by the PID controller, not by the function generator that produces the scan signal.

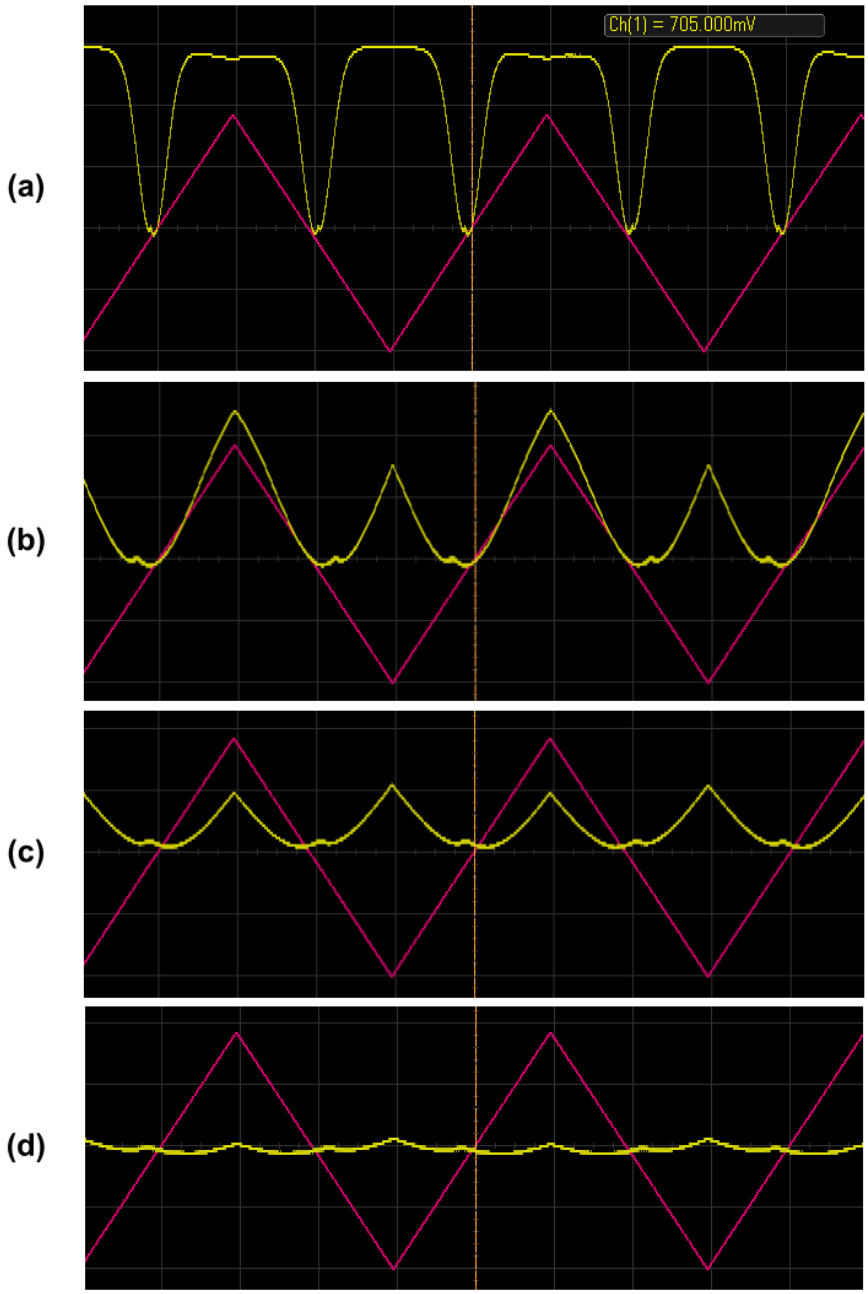

Chapter 5

Phase Lock

5.1 Motivation for the Phase Lock

The 689 nm laser is poised to serve as the oscillator for an atomic clock, with its performance determined by the rate and uniformity of oscillation. While the 689 nm laser exhibits a lower oscillation rate compared to the 461 nm laser, its primary advantage lies in the stability attainable by locking it to the $^1S_0$-$^3P_1$ transition. As previously noted, the $^1S_0$-$^3P_1$ transition boasts a significantly narrower linewidth ($\Gamma = 2\pi \times 7.6$ kHz) than the $^1S_0$-$^1P_1$ transition ($\Gamma = 2\pi \times 32$ MHz). While this slender linewidth promises considerable benefits once the 689 nm laser is locked to the transition, it also poses a challenging obstacle to surmount.

The exceptional narrowness of the $^1S_0$-$^3P_1$ transition presents a significant challenge in attaining resonance with the 689 nm laser. Environmental factors, such as temperature fluctuations, acoustic vibrations, and air pressure variations, may introduce noise that impedes the laser's ability to achieve resonance with the transition. Furthermore, the spin-forbidden nature of the $^1S_0$-$^3P_1$ transition results in a substantially lower absorption probability for resonant photons compared to those resonating with the intermediate transition. These factors contribute to the considerable difficulty in measuring the absorption of this transition, and consequently, in difficulty employing an absorption frequency-lock technique for the 689 nm laser analogous to the frequency-lock detailed in Chapter 4. To overcome this challenge and enhance the stability of the 689 nm laser, it is necessary to implement a phase lock, enabling the accurate measurement of absorption on the $^1S_0$-$^3P_1$ transition.

A phase lock offers greater precision compared to a frequency lock due to the requirement that the frequencies of the laser and the reference must already be matched or resonant with one another. Employing a principle akin to that of a frequency lock, a phase lock involves mixing a reference signal with an input signal, generating a DC error signal, and subsequently processing the error signal through a PID controller to regulate the laser's output. However, in a phase lock, the reference and input signals are not presumed to be in phase; rather, their frequencies are assumed to be identical. Consequently, the generated error signal is exclusively based on the phase difference between the two frequencies.

5.2 Phase Lock Theory

Consider an input signal represented by Equation 5.1 and a reference signal represented by Equation 5.2:

$$V_{in} = A\sin(2\pi f_{in}t + \phi_{in}) \tag{5.1}$$

$$V_r = B\sin(2\pi f_r t + \phi_r) \tag{5.2}$$

Assuming $f_r = f_{in}$, combining the input and reference signals yields a mixer output described by Equation 5.6:

$$V_{mixed} = V_{in} \times V_r \tag{5.3}$$

$$= A\sin(2\pi f_{in}t + \phi_{in}) \times B\sin(2\pi f_r t + \phi_r) \tag{5.4}$$

$$= A\sin(2\pi f_r t + \phi_{in}) \times B\sin(2\pi f_r t + \phi_r) \tag{5.5}$$

$$V_{mixed} = \frac{AB}{2}[\cos(\phi_{in} - \phi_r) - \cos(4\pi f_r t + \phi_{in} + \phi_r)] \tag{5.6}$$

Disregarding the second term in Equation 5.6, it becomes evident that a DC component is generated solely due to the phase difference between the input and reference signals, as illustrated in Equation 5.7:

$$V_{mixed} = \frac{AB}{2}\cos(\phi_{in} - \phi_r) \tag{5.7}$$

When the input and reference signals are in phase, the DC component of the mixer output is zero. However, if these signals are not in phase, the DC component of the mixer output becomes non-zero. This non-zero DC output is subsequently employed by a PID controller in a manner analogous to the error signal used in the frequency lock, adjusting the output of the 689 nm laser to align in-phase with the reference signal.

5.3 Phase Lock System

As illustrated in Figure 5.1, the phase lock system consists of three primary components. Firstly, a beat note is generated from the light emitted by the 689 nm laser and the frequency comb (refer to Chapter 1 for beat note generation details). Secondly, the photodiode output undergoes a series of filtering processes to isolate a beat note near 160 MHz for use in the phase lock. Thirdly, the beat note and a reference frequency at 160 MHz are mixed to produce a DC error signal, which is subsequently employed by a PID controller to adjust the 689 nm laser output and align it in-phase with the reference frequency. The photodiode output, prior to frequency filtering, is depicted in Figure 5.2.

The frequency on the right side of Figure 5.2 represents the frequency comb's repetition rate, which is locked at 250 MHz. The central frequency in Figure 5.2 corresponds to the beat note utilized for the phase lock of the 689 nm laser. This beat note is manually adjusted to be within 5 MHz of 160 MHz, ensuring that the beat note and reference frequencies are sufficiently similar to facilitate the phase lock.

To guarantee that the generated error signal is attributable to the beat note near 160 MHz, the photodiode output is subjected to a series of low-pass and high-pass filters. As shown in Figure 5.1, these filters yield the output signal presented in Figure 5.3.

The filters effectively suppress the repetition rate and the smaller beat note from the pho-

Figure 5.1: Phase Lock System. M = Mirror; Iso = Optical Isolator; HWP = Half Wave Plate; FP = Fiber Port; FS/C = Fiber Splitter/Coupler; Exp = Optical Expander; PD = Photodiode; LP = Low-Pass Filter; HP = High-Pass Filter; C/S = Electronic Coupler/Splitter; DM = Digital Mixer; FG = Function Generator; PID = Proportional–Integral–Derivative; Att = Electrical Attenuator.

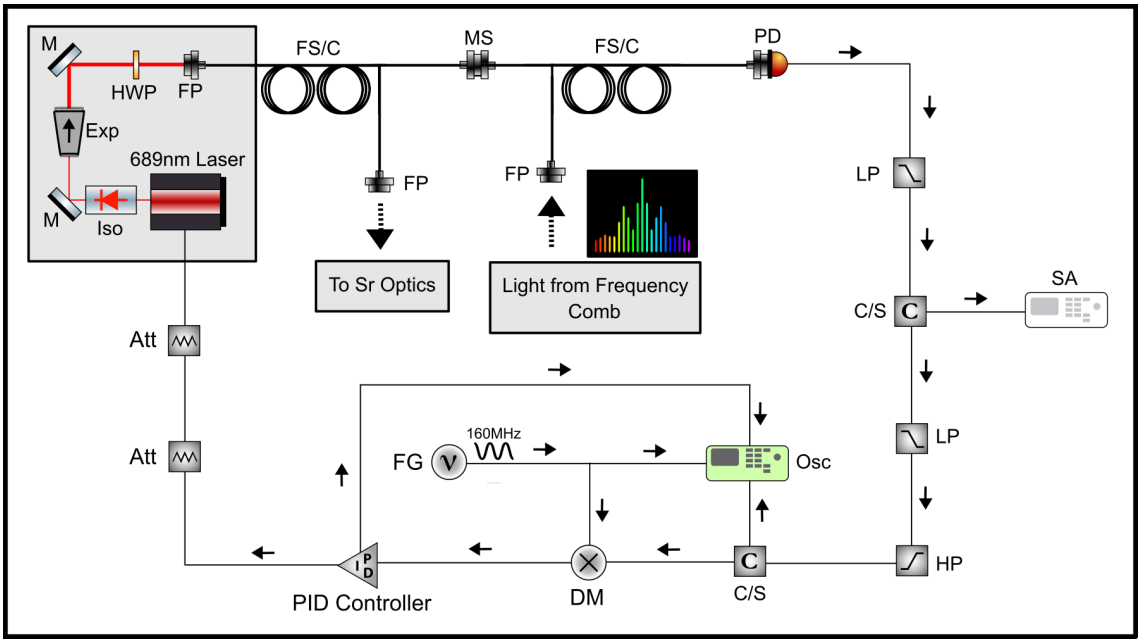

Figure 5.2: The x-axis measures frequency, while the y-axis measures voltage in units of dBm.

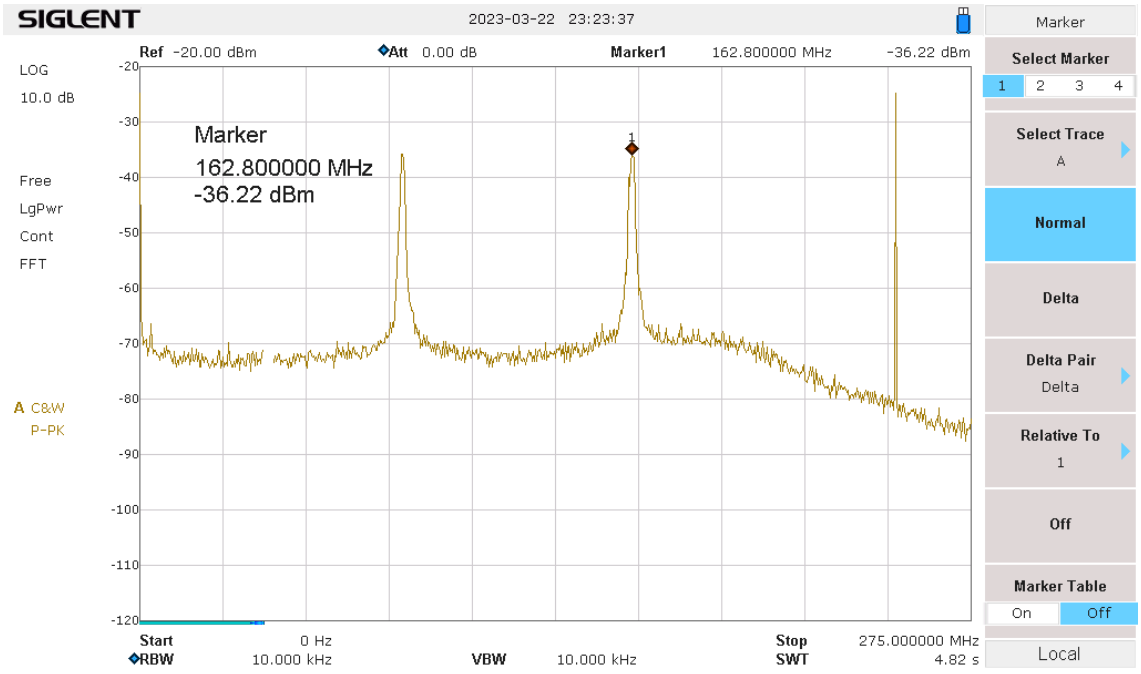

Figure 5.3: Filtered Beat Note.

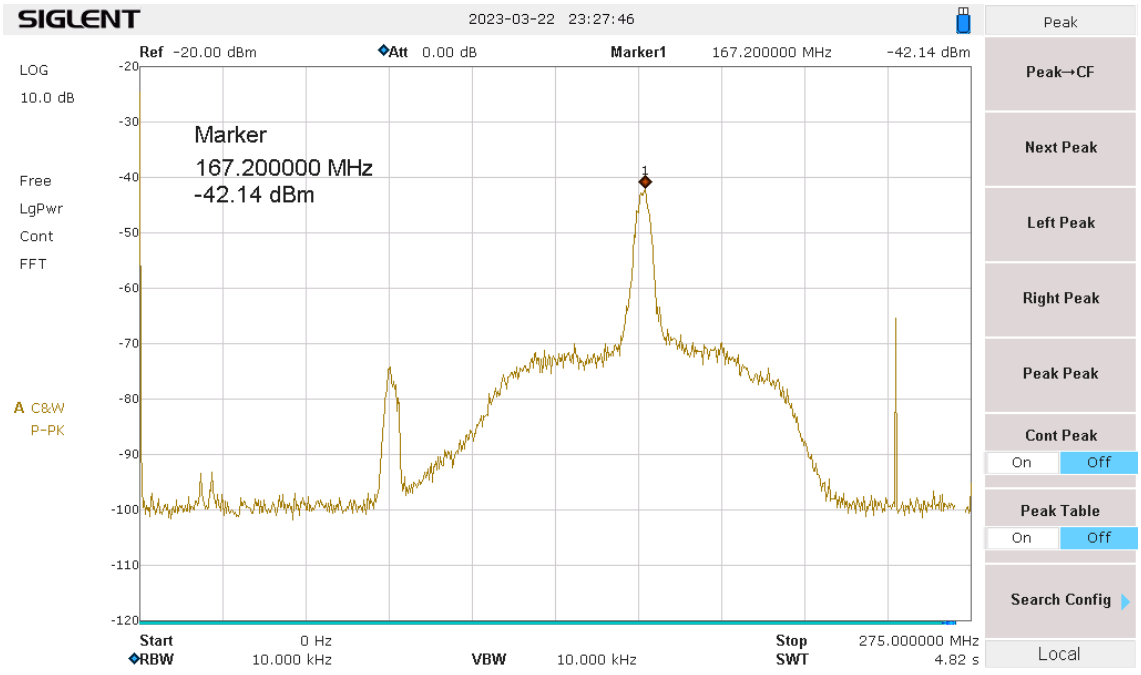

todiode output, causing the DC signal produced by the mixer to be dominated by the beat note near 160 MHz. This DC signal is utilized by the PID controller depicted in Figure 5.1 to adjust the 689 nm laser output, ensuring coherence with the reference signal. When the 689 nm laser is phase-locked to the 160 MHz reference, the beat note begins to resemble a delta function at the reference frequency. Figure 5.4 displays the beat note when the laser is locked, while Figure 5.5 presents the waveform of the reference and the beat note when the 689 nm laser is locked.

The reduced noise of the 689 nm laser due to the phase lock may eventually allow for measurable absorption of the $^1S_0$-$^3P_1$ transition. Subsequently, a clock can be established by frequency-locking the 689 nm laser light so that it resonates with the transition. Since the locked beat note lies within the radio frequency range, the oscillations of the beat note can be counted. The frequency of the 689 nm laser light can then be precisely determined using Equation 5.8, where f_l represents the laser frequency, f_{CEO} denotes the carrier-envelope offset of the frequency comb, f_{rep} refers to the repetition rate of the frequency comb, n indicates the integer number of the comb tooth employed to generate the beat note, and f_b corresponds to the beat note frequency.

$$f_l = f_{CEO} + n f_{rep} + f_b \tag{5.8}$$

Figure 5.4: Locked Beat Note: Signal Analyzer. This signal is generated by the beat note signal near 160 MHz when the PID controller is activated.

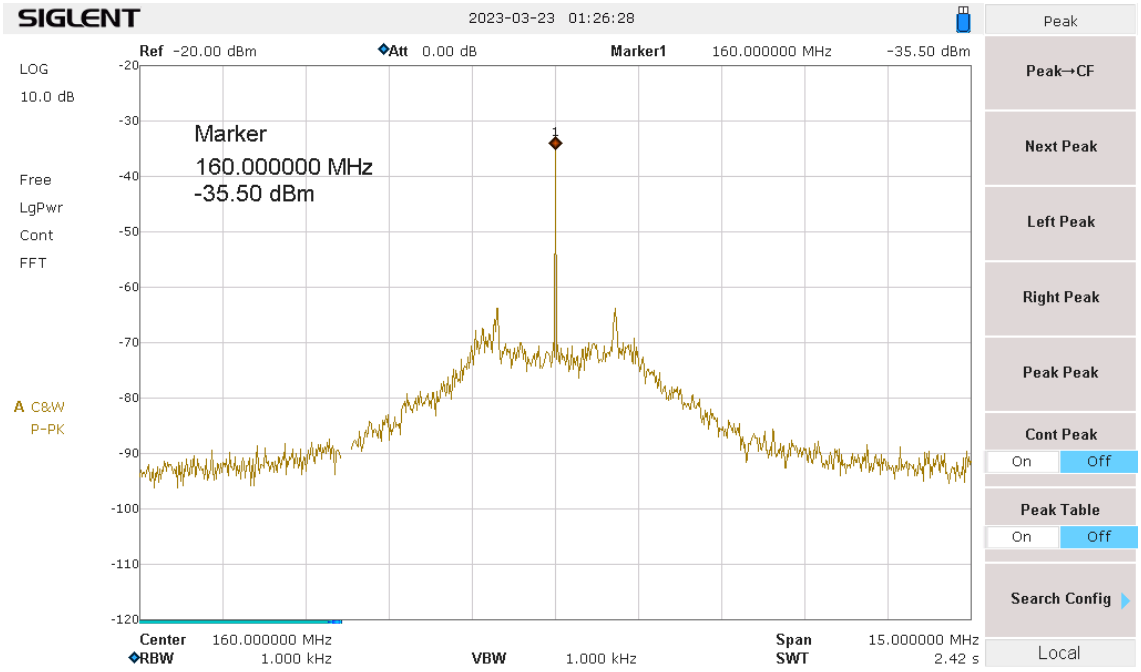

Figure 5.5: Locked Beat Note: Oscilloscope. The 160 MHz reference signal is represented by the yellow curve, while the beat note signal is displayed by the green curve. The two signals exhibit a minimal phase difference. The "haziness" of the beat note originates from the 689 nm laser noise that has not yet been mitigated.

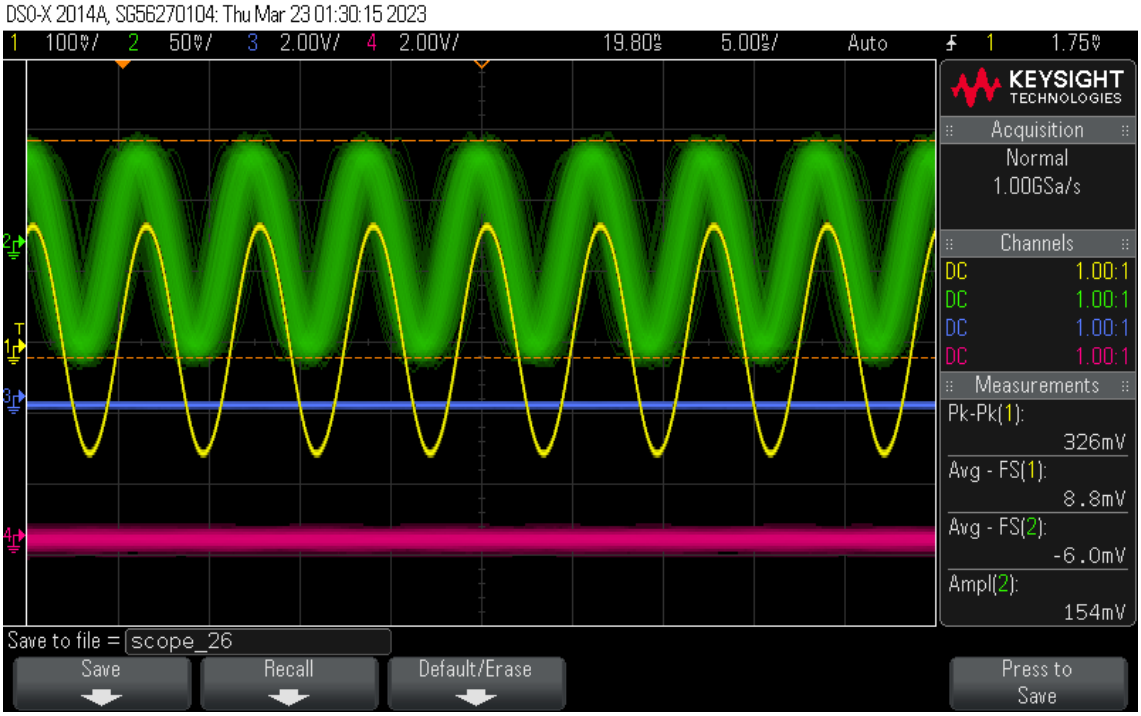

Chapter 6

Conclusion

As it stands, a clock has not yet been developed using the shelving spectroscopy scheme described in this paper, mainly due to multiple issues related to the quality of the error signal for each locking system.

6.1 Current Status of the Frequency Lock

Although the frequency lock can lock the 461 nm laser to the $^1S_0$-$^1P_1$ transition, the lock's quality is inadequate for measuring the absorption of the 689 nm laser. This is primarily attributed to an abnormality in the error signal generated by the tandem LIA system. This abnormality arises because the Doppler-free feature created by the pump beam of the 461 nm laser does not precisely coincide with the local minimum of the absorption profile, as illustrated in Figure 6.1. Consequently, a non-zero error signal is produced by the tandem LIA system even if the 461 nm laser is resonant with the $^1S_0$-$^1P_1$ transition. This is due to the fact that if the 461 nm laser is resonant with the local minimum of the absorption profile, a non-zero error signal is generated by the Doppler-free feature. Conversely, if the 461 nm laser is resonant with the Doppler-free feature, a non-zero error signal is generated by the local minimum of the absorption profile. This results in the error signal reaching 0V between these two features at a frequency that is not optimally resonant with the transition.

One hypothesis for the misalignment between the Doppler-free feature and the local minimum of the absorption profile is that there might be a relationship between the intensity of the laser

light emitted by the 461 nm laser and the current of the laser during its scan. Since the absorption of the $^1S_0$-$^1P_1$ transition is measured by the transmission of the 461 nm laser light through the strontium sample, fluctuations in the laser light's intensity over the 5 Hz scan might prevent the local minimum of the absorption profile from accurately indicating the frequency resonant with the transition.

Another potential explanation for the offset between the Doppler-free feature and the local minimum of the absorption profile is that the AOM used to supply the 30 kHz dither for the pump beam in the saturation absorption scheme shifts the frequency of the pump beam. This would result in the pump and probe beams having different frequencies, thereby creating a Doppler-free feature offset from the resonance frequency.

The quality of the error signal produced by the tandem LIA system is also constrained by the signal strength of the Doppler-free feature. Figure 6.2 illustrates the difference in signal strength between the absorption profile of the 5Hz scan and the Doppler-free feature. Enhancing the magnitude of the Doppler-free feature would improve the quality of the error signal generated by the second LIA in the tandem LIA system.

6.2 Potential Improvements of the Frequency Lock

The quality of the frequency lock might be enhanced by increasing the temperature at which the strontium sample is heated. Figure 6.3 displays the absorption profile of the sample when it is near 370 K, rather than the 470 K at which the sample is heated to produce the absorption profile in Figure 6.2. It is evident that there is a relationship between the scan signal, shown in pink, and the absorption profile, shown in yellow that is not due to absorption of the 461 nm light by the strontium sample. Observing Figure 6.2, which presents the absorption profile for the sample near 470 K, this relationship between the scan and the absorption can still be seen near the local maximums of the absorption profile. This suggests that the sample is inadequately heated at 470 K, and heating the sample further may improve both the local minimum and the Doppler-free feature. Enhancing the signal clarity of each of these features will reduce noise on the signal output,

Figure 6.1: Doppler-free Feature Offset.

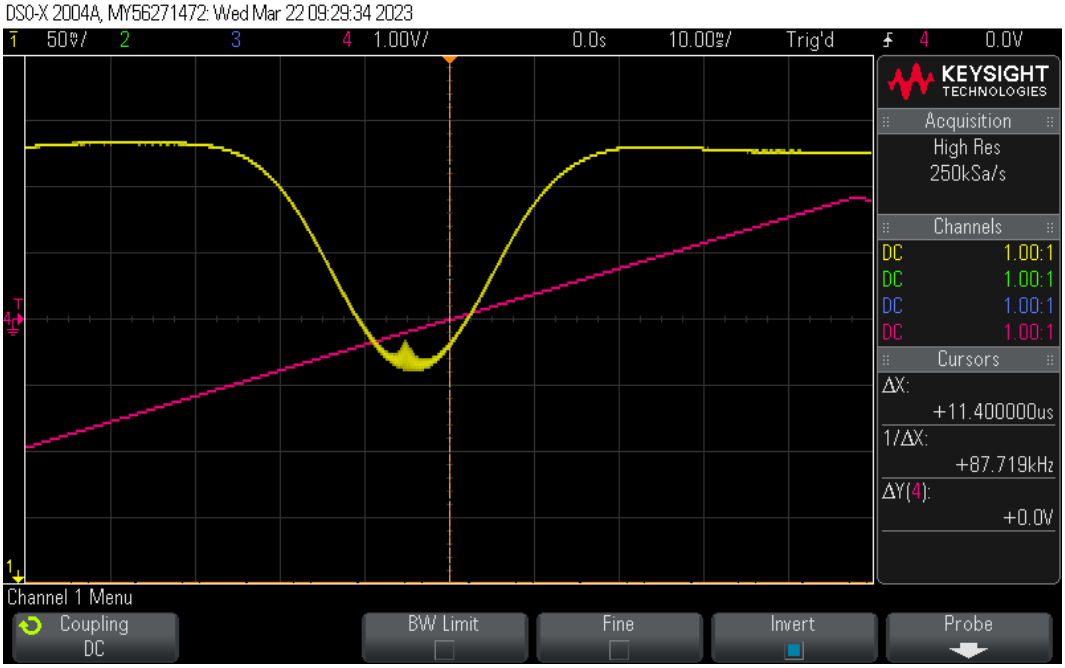

Figure 6.2: Absorption Profile Compared to Doppler-free Feature

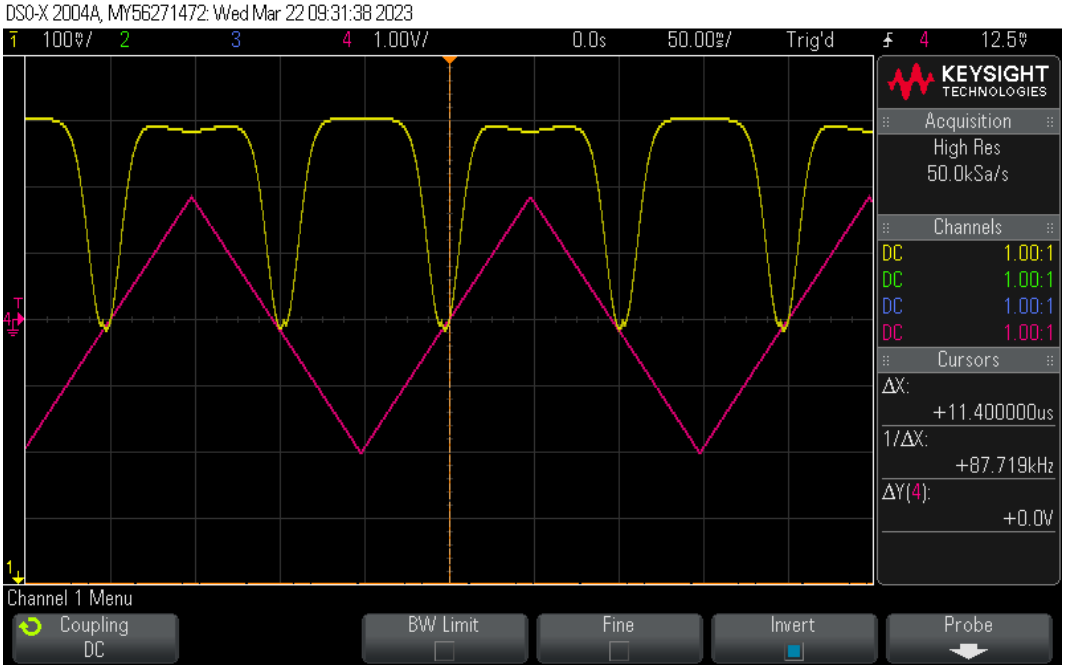

ultimately leading to an improved error signal generated by the tandem LIA system.

6.3 Current Status of the Phase Lock

The phase lock can lock the 689 nm laser to the 160 MHz reference frequency. However, a significant amount of light produced by the 689 nm laser is not adequately locked. Figure 6.4 shows the signal analyzer output of the 160 MHz beat note when the phase lock is activated. A portion of the light is coherent with the 160 MHz reference, but a substantial proportion of the light produced generates beat note signals at ±10 MHz from 160 MHz. This indicates that a measurable part of the output of the 689 nm laser is not locked. This situation would be acceptable if the intensity of the locked portion were higher. However, since the light from the 689 nm laser needs to be divided for use in both the phase lock and the shelving spectroscopy scheme, the intensity of the locked light is not sufficient for measuring the absorption of the $^1S_0$-$^3P_1$ transition.

6.4 Potential Improvements of the Phase Lock

The potential enhancements for the phase lock involve increasing the intensity of the laser without exacerbating the frequency noise of the 689 nm laser. One approach for improvement is to refine the error signal generated by the mixer in the phase lock. A possible method to achieve this is by incorporating a low-pass filter below 320 MHz between the digital mixer and the PID controller in Figure 6.5. This will attenuate the AC signal generated by the mixer, thereby producing a purely DC error signal that the PID controller can use to adjust the 689 nm laser. The inclusion of a 320 MHz low-pass filter addresses a relatively minor oversight discovered during the writing of this paper.

Another potential enhancement for the output of the phase lock is to increase the intensity of the light used in the shelving spectroscopy scheme without necessarily improving the phase lock itself. One way to augment the intensity of the 689 nm light used for spectroscopy is to first send the light through an injection scheme. An injection scheme involves a laser diode that is close to the frequency of the 689 nm light. By directing the 689 nm light into the laser diode before

Figure 6.3: Absorption Profile of Insufficiently-heated Sample.

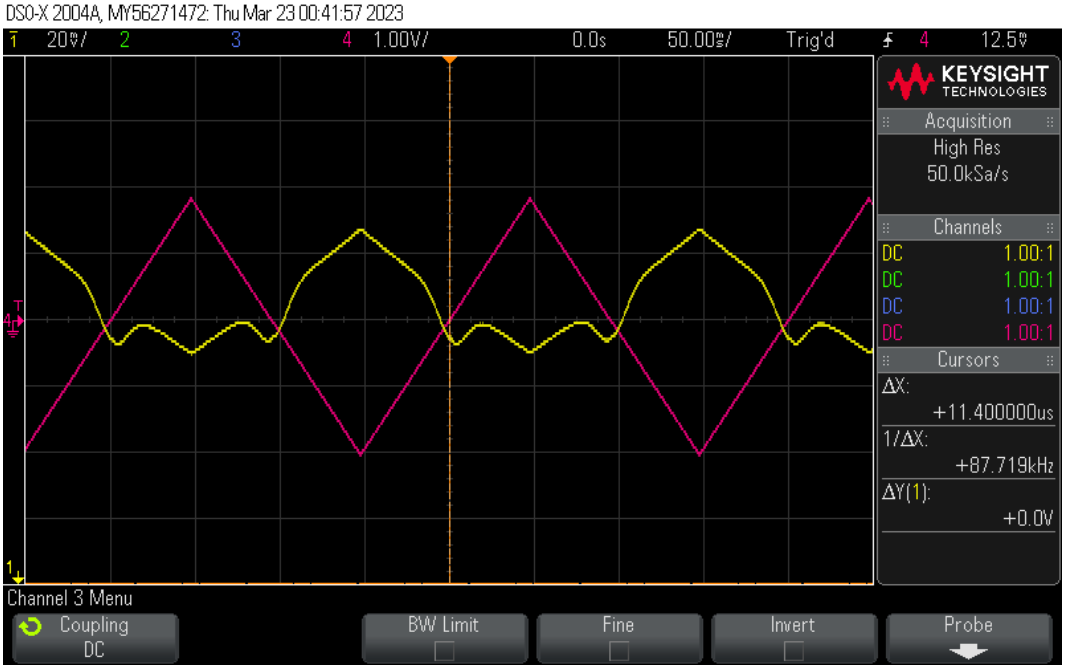

Figure 6.4: Phase Locked Beat note.

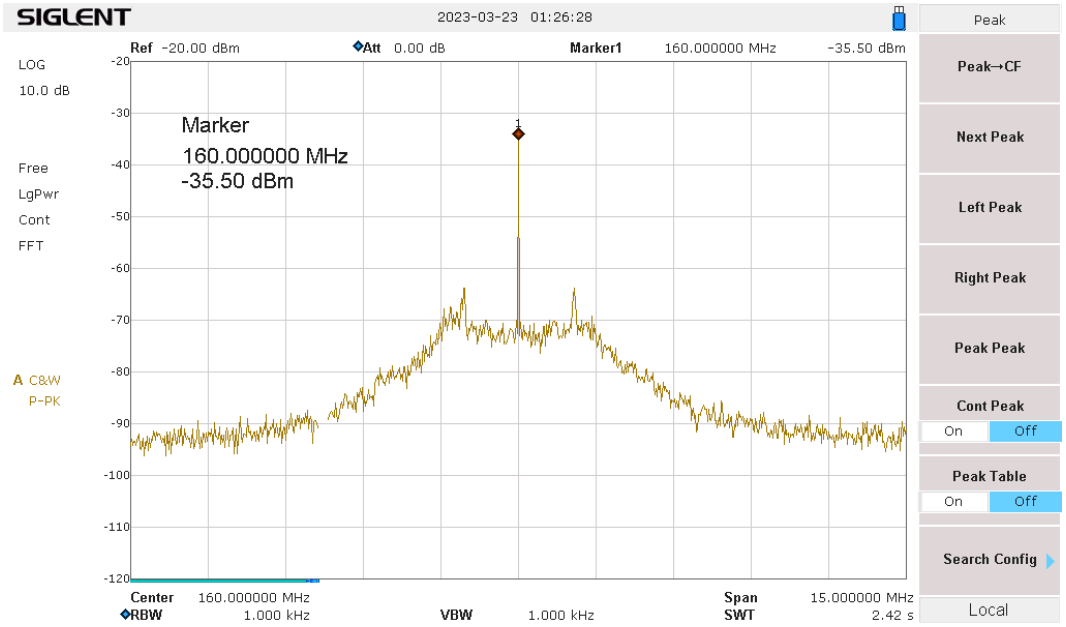

Figure 6.5: Phase Lock Diagram. M = Mirror; Iso = Optical Isolator; HWP = Half Wave Plate; FP = Fiber Port; FS/C = Fiber Splitter/Coupler; Exp = Optical Expander; PD = Photodiode; LP = Low-Pass Filter; HP = High-Pass Filter; C/S = Electronic Coupler/Splitter; DM = Digital Mixer; FG = Function Generator; PID = Proportional–Integral–Derivative; Att = Electrical Attenuator.

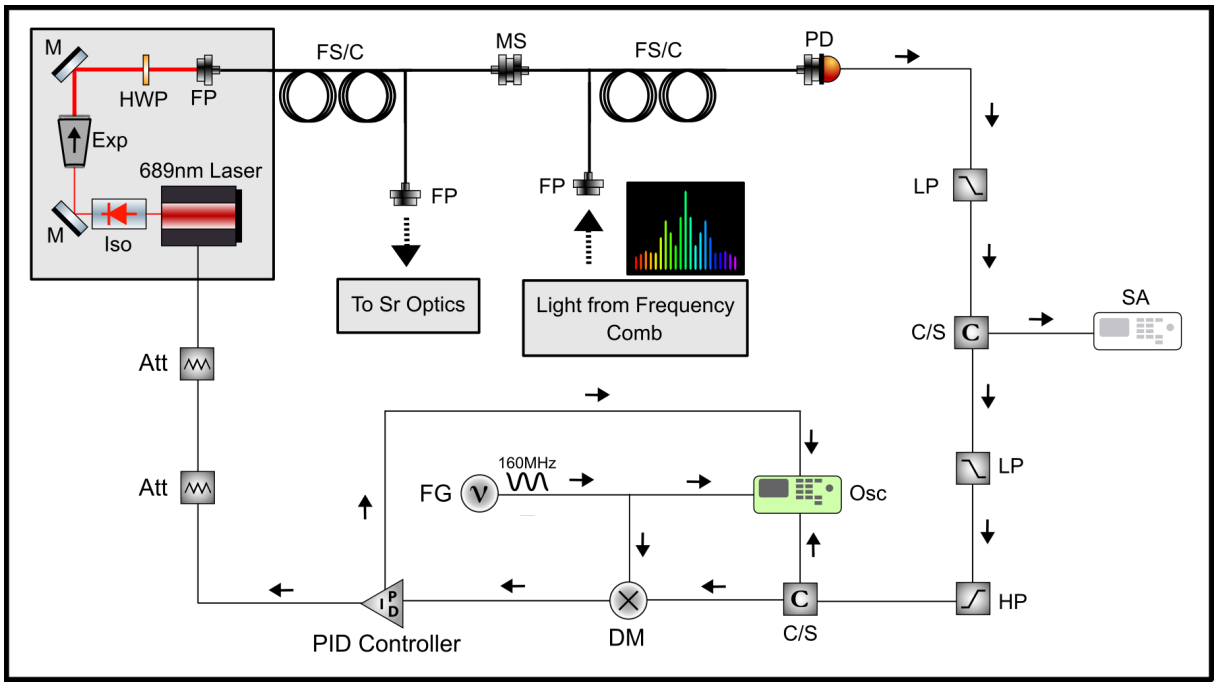

spectroscopy, it is possible to increase the intensity of the light without introducing additional noise to the frequency of the output [3].

6.5 Next Steps for Clock Development

The following steps must be completed to develop an atomic clock using a micro-fabricated vapor cell and the $^1S_0$-$^3P_1$ strontium transition. First, the frequency and phase locks need to be enhanced, potentially using the suggestions outlined in this chapter. Second, a frequency lock system must be devised between the 689 nm laser and the shelving spectroscopy measurement of the absorption of the $^1S_0$-$^3P_1$ transition.

Once both of these steps have been achieved, a clock is created by pairing the 689 nm laser's beat note with an RF frequency counter. The precise frequency of the laser can then be calculated using Equation 6.1.

$$f_l = f_{CEO} + n f_{rep} + f_b \tag{6.1}$$

Counting the oscillations of the beat note effectively converts the abstract quantity of time into a measurable physical quantity.

Bibliography

[1] Mitsuru Asano and Kenji Kubo. Vapor pressure of strontium below 660°k. J. Nucl. Sci. Technol., 15(10):765–767, October 1978.

[2] B J Bloom, T L Nicholson, J R Williams, S L Campbell, M Bishof, X Zhang, W Zhang, S L Bromley, and J Ye. An optical lattice clock with accuracy and stability at the 10(-18) level. Nature, 506(7486):71–75, feb 2014.

[3] V Bolpasi and W von Klitzing. Double-pass tapered amplifier diode laser with an output power of 1 W for an injection power of only 200 μW. Rev. Sci. Instrum., 81(11):113108, November 2010.

[4] T Dyer, S J Ingleby, C Dunare, K Dodds, P Lomax, P F Griffin, and E Riis. Micro-fabricated caesium vapor cell with 5 mm optical path length. J. Appl. Phys., 132(20):204401, November 2022.

[5] EurekAlert! Ultraprecise atomic clock poised for new physics discoveries, feb 2022.

[6] Rudy Fuks. SMA Connectors with Extended Frequency Range, 2007.

[7] Jose M. Juarez. The use of a lock-in amplifier to stabilize the frequency of a laser diode. Bachelor's thesis, College of the Holy Cross, 2009. Honor's Thesis.

[8] S. Knappe, V. Gerginov, P. D.D. Schwindt, V. Shah, H. G. Robinson, L. Hollberg, and J. Kitching. Atomic vapor cells for chip-scale atomic clocks with improved long-term frequency stability. Opt. Lett., 30(18):2351–2353, Sep 2005.

[9] S. Knappe, V. Velichansky, H.G. Robinson, L. Liew, J. Moreland, J. Kitching, and L. Hollberg. Atomic vapor cells for miniature frequency references. In IEEE International Frequency Control Symposium and PDA Exhibition Jointly with the 17th European Frequency and Time Forum, 2003. Proceedings of the 2003, pages 31–32, 2003.

[10] Svenja Knappe, V Shah, Peter Schwindt, Leo Hollberg, John Kitching, Li-Anne Liew, and John Moreland. A microfabricated atomic clock. (85), 2004-01-01 2004.

[11] Thomas Legero, J. S. Raaj Vellore Winfred, Fritz Riehle, and Uwe Sterr. Ultracold 88sr atoms for an optical lattice clock. pages 119 – 122, 05 2007.

[12] Li-Anne Liew, Svenja Knappe, John Moreland, Hugh Robinson, Leo Hollberg, and John Kitching. Microfabricated alkali atom vapor cells. Appl. Phys. Lett., 84(14):2694–2696, April 2004.

[13] I Manai, A Molineri, C Fréjaville, C Duval, P Bataille, R Journet, F Wiotte, B Laburthe-Tolra, E Maréchal, M Cheneau, and M Robert-de Saint-Vincent. Shelving spectroscopy of the strontium intercombination line. J. Phys. B At. Mol. Opt. Phys., 53(8):085005, April 2020.

[14] E H Martin, A Zafar, J B O Caughman, R C Isler, and G L Bell. Applications of doppler-free saturation spectroscopy for edge physics studies (invited). Rev. Sci. Instrum., 87(11):11E402, nov 2016.

[15] Hitoshi Nishino, Yasubumi Furuya, and Takahito Ono. Micro vapor cells sealed by two-step bonding for miniature atomic clocks. jul 2021.

[16] NIST. JILA strontium atomic clock sets new records in both precision and stability, jan 2014.

[17] NIST. NIST Team Demonstrates Heart of Next-Generation Chip-Scale Atomic Clock, may 2019.

[18] Clément Paradis. Novel Ultrafast High-Power Thin-Disk Laser Oscillators and Applications for Metrology and XUV Generation. PhD thesis, Université de Neuchâtel, 12 2017.

[19] M Schioppo, N Poli, M Prevedelli, St Falke, Ch Lisdat, U Sterr, and G M Tino. A compact and efficient strontium oven for laser-cooling experiments. Rev. Sci. Instrum., 83(10):103101:1–6, October 2012.

[20] Bonnie L Schmittberger and David R Scherer. A review of contemporary atomic frequency standards. 2020.

[21] R Straessle, M Pellaton, C Affolderbach, Y Pétremand, D Briand, G Mileti, and N F de Rooij. Microfabricated alkali vapor cell with anti-relaxation wall coating. Appl. Phys. Lett., 105(4):043502, July 2014.

[22] Wikipedia. Carrier-envelope phase, sep 2020.

Appendix A

Equations

$$(1)\ \text{Maximum Fractional Frequency Deviation} = \frac{\text{Transition Linewidth}}{\text{Transition Frequency}}$$

$$(2)\ \text{Comparative Precision} = \frac{\text{Maximum Fractional Frequency Deviation for 1st Transition}}{\text{Maximum Fractional Frequency Deviation for 2st Transition}}$$

$$(3)\ \text{MCD (Years)} = \frac{\text{TF}}{\text{TL} \times \text{SPY}},$$

MCP = Minimal Clock Peviation, i.e. Minimum number of years for clock to deviate by 1 second,

TF = Transition Frequency,

TL = Transition Linewidth,

SPY = Seconds Per Year or 31,536,000 seconds.